공학박사 학위논문

Development of a Multigroup Cross Section Generator for Fast Reactor Analysis Directly Employing Evaluated Nuclear Data Files

평가핵자료집 직접 처리를 통한 고속로 해석용

다군 핵단면적 생산기 개발

2018년 2월

서울대학교 대학원

에너지시스템 공학부 원자핵공학 전공

임 창 현

Development of a Multigroup Cross Section Generator for Fast Reactor Analysis Directly Employing Evaluated Nuclear Data Files

평가핵자료집 직접 처리를 통한 고속로 해석용 다군 핵단면적 생산기 개발

지도 교수 주 한 규

이 논문을 공학박사 학위논문으로 제출함

2018년 2월

서울대학교 대학원

에너지시스템공학부

임 창 현

임창현의 공학박사 학위논문을 인준함

2018년 2월

위 원 장 심 형 진 (인)

부위원장 주 한 규 (인)

위 원 김 응 수 (인)

위 원 김 상 지 (인)

위 원 이 영 욱 (인)

Abstract

A fast reactor multigroup XS generation code, EXUS-F is developed that is capable of directly processing the ENDF format nuclear data libraries based on various detailed spectrum calculations. The RECONR module of NJOY is used to generate pointwise cross section data and the Doppler broadening of the major heavy nuclides is incorporated by the Gauss-Hermite quadrature method. An ultrafine group structure consisting of 2123 energy groups ranging upto 20 MeV is employed for the spectrum calculation and the structure can be adjusted by the user input. The self-shielding effect is incorporated in the ultrafine group cross section by a numerical integration scheme based on the narrow resonance approximation. For the self-shielding in the unresolved resonance range, the probability table method is proposed that employs the probability table library generated by the NJOY PURR module. The functions to generate fission spectrum matrices and scattering transfer matrices directly from the nuclear data library are realized. The extended transport approximation is used in the zero-dimensional (0D) calculation to obtain higher order moment spectra and the Collision Probability (CP) method and the MOC method with the higher order scattering source are employed selectively for one-dimensional (1D) cylinder and two-dimensional (2D) hexagon calculations.

Verification calculations are performed for homogenous mixture and cylindrical problems. The results are assessed by comparing with the McCARD Monte Carlo solutions and it is confirmed that the spectrum calculations and the corresponding multigroup cross

section generations are performed adequately in that the reactivity error is less than 60 pcm. The EXUS-F/nTRACER calculation is performed in a 47 group structure for the two-dimensional ABR 1000 benchmark using ENDF/B-VII.0. The reactivity error of 260 pcm and the root mean square error of the pin powers of 1.1% indicate that EXUS-F generates properly the broad group cross sections for the nTRACER fast reactor calculations. Results obtained using JENDL and ENDF/B-VII.1 are obtained with those of ENDF/B-VII.0 showing no significant differences.

Keywords : multigroup cross section
fast reactor
ultrafine group
ENDF format
ABR 1000 benchmark
Student Number : 2012-30964

Contents

List of Tables

List of Figures

Chapter 1. Introduction

Currently most nuclear reactor analyses are performed employing the conventional two-step procedure in which assembly homogenized broad group cross sections are generated at the first step for use in the low order whole core calculation at the second step. The two-step procedure has inherent limitations in accuracy because the neutron flux spectra and distribution obtained at the first step are different from the actually observed ones in the core due to the fact that small geometries are used at the first step. The approach of direct whole core calculation was proposed recently to remove the approximations involved in the two-step procedure by explicitly representing the geometry and materials and by keeping the detailed energy structure. This approach requires considerably more computing resource than the two-step procedure and becomes increasingly more practical with the growth in high performance computing. The nTRACER[1] code of Seoul National University (SNU) is one of the codes to perform direct whole core calculation for light water reactors (LWRs).

Along the development of the Prototype Generation-IV Sodium cooled Fast Reactor (PGSFR)[2] of Korea Atomic Energy Research Institute (KAERI), a program to develop a new computer code system for fast reactor analysis was initiated at Korea Institute of Nuclear Safety (KINS) to obtain higher fidelity solutions. As a part of the program, it was planned to extend the capability of the direct whole core calculation code nTRACER for applications to fast reactor analyses with pin-level resolution. For this extension, a new multigroup (MG) fast reactor cross section (XS) library is required which should be produced through a unique generation procedure that is totally different from that for LWRs. This is because fast reactors have very distinctive characteristics which are significantly different from those of LWRs[3].

Generation of MG XS library starting from the evaluated

nuclear data files is one of the most important processes in reactor analyses since it is not possible to achieve sufficient accuracy in the reactor calculation without using proper MG XSs. In the traditional MG XS generation procedure for fast reactor analysis, the Bondarenko self-shielding factor method[4] was used. In this method, a MG XS library is pre-calculated in a broad group structure (~100 groups) based on the neutron spectra of a specific fast reactor core as functions of energy and temperature. Thus inevitable errors are introduced in the core calculation results if the spectra of the target core are significantly different from the base spectra. An alternative approach[5] was proposed to calculate MG XSs based on detailed spectrum calculations for specific compositions by Argonne National Laboratory (ANL) with the ultrafine group (UFG) structure (~2000 groups). It has an advantage of detailed energy modeling employing the UFG structure, but the self-shielding calculations for UFG XSs are complex and have some limitations. In recently developed codes, the limitation of the Bondarenko self-shielding factor method was also resolved by introducing the UFG structure and performing the detailed spectrum calculations[6,7]. An improved self-shielding method for the UFG structure of the ANL method was developed using the numerical integration scheme[8].

The goal of this work is to develop a MG XS generator to provide proper MG XS sets for fast reactor direct whole core calculations by nTRACER with pin-level resolution by employing the up-to-date methods and by devising new methods needed for the efficient direct use of the Evaluated Nuclear Data File (ENDF) format nuclear data files. Since ENDF data files and the NJOY system[9] are publicly available and are updated once in a while, it would be beneficial to construct a fast reactor MG XS generation code that directly accesses the ENDF format raw nuclear data so that core specific MG XS libraries are generated readily without any intermediate steps. This benefit provides the basic motivation for this work that encompasses a lot of involved steps in the effective XS generation, scattering matrix calculation considering anisotropy, slowing down calculation and etc. In the following, previous

researches in the area of fast reactor MG XS generation are reviewed in more detail at first and the objectives and scopes of this work are given.

1.1. Previous Researches

In 1970s, the Bondarenko self-shielding factor method[4] was widely used in the MG XS generation for fast reactor analysis. Bondarenko introduced the concept of background XS by separating the macroscopic total XS in a homogenous medium into two terms: the first term for the total XS of the target isotope and the second term that encompasses all of the other isotopes in the mixture. He then represented the MG XS of the target isotope as a function of background XS. The concept of background XS was extended to heterogeneous media by introducing the effective escape XS. With this, the Bondarenko self-shielding factor method can handle a heterogeneous medium in the same manner as homogenous media. The method was employed in many typical codes[9,10,11].

In this method, a generalized MG XS library[12,13,14] is prepared which contains the self-shielded XSs as functions of background XS and temperature. Then the background XS is calculated for the composition of a material and the self-shielded XS for the composition is interpolated using the tabularized function of the generalized MG XS library. The self-shielded XSs in the library are, however, determined using the neutron spectra of a specific fast reactor core which are used as the weighting functions in the energy condensation process. Thus nontrivial errors are introduced in the core calculation results if the spectra of the target core deviate a lot from the base spectra. There is also a limitation in the incorporation of the resonance interference effects of the intermediate mass nuclides such as ^{52}Cr, ^{56}Fe which have resonance-like XSs in the fast energy range because of the broad group structure.

In fast reactor spectra, most neutrons appear in the keV and

MeV energy range because of the small slowing down power. Thus the energy ranges of fission neutrons and neutrons inducing fission mostly overlap. The small slowing down power also eliminates the 1/E spectrum noted in the LWRs. The spectrum rapidly decreases with decreasing energy. Resonance scattering XSs of the intermediate mass nuclides make jagged structure in the fast reactor spectrum. Due to these factors, fast reactor spectrum calculations for the MG XS generation require more detailed energy modeling compared with the Bondarenko self-shielding factor method. For these reasons, a method employing detailed neutron spectrum calculations was proposed by a group at ANL and it was implemented in the ETOE-2/MC^2-2/SDX code system[5]. The ultrafine group structure with a constant group width, 1/120 in lethargy, was initially introduced and the structure is widely used in the recently developed codes for fast reactor MG XS generation. It performs the transport calculation with the UFG structure consisting of 2082 groups with the constant lethargy width spanning from 0.4 MeV to 14.19 eV. In this method, the UFG XSs are prepared by performing resonance self-shielding calculations using the analytic resonance integral method for the resolved and unresolved resonance ranges and pre-calculated UFG XSs are given for other energy ranges. The ANL method of MC^2-2 has an advantage of detailed energy modeling by introducing the UFG structure. In the resonance self-shielding calculation using the analytic resonance integral method, however, the resonance tail effect is pronounced with the UFG structure for the resonances lying across a group boundary.

Recently MC^2-3[8] was developed at ANL by improving the resonance self-shielding and spectrum calculations of MC^2-2. It introduced the numerical integration approach for resonance self-shielding estimation using the Narrow Resonance (NR) approximation. In this method, the self-shielded UFG XS is determined by a numerical integration using the pointwise XSs. It is a very simple method compared to the analytic resonance integral method. Yet it allows great improvement in the accuracy of

resonance self-shielding including resonance interference effects. MC^2-3 also provides a HFG calculation capability for more rigorous energy treatment.

The ECCO[6] code of CEA and the SLAROM-UF[7] code of JAERI improved the self-shielding factor method by utilizing more energy groups. ECCO performs slowing down calculations based on various multi-dimensional lattice calculation capabilities with the fine group structure (1968 groups) for the most important nuclides and the broad group structures (33 groups or 172 groups) for less important nuclides. The group width of the fine group structure of ECCO is the same as the UFG width of MC^2-2. However, the resonance self-shielding treatment is handled by applying the subgroup method of ECCO. SLAROM-UF performs slowing down calculations with the ultrafine group structure which has the same lethargy width of 1/120 for the energy range above 52.5 keV. Hyperfine group calculations (~100,000 groups) are carried out for the range below 52.5 keV to treat resonance structures directly. In the UFG group calculation, the self-shielding effect is considered using the Bondarenko self-shielding factor method only for heavy nuclides having resonances above 52.5 keV.

1.2. Purpose of Research

Aforementioned three recent codes to generate the MG XSs for fast reactor analysis have significant differences not only in the resonance self-shielding method, but also in the multi-dimensional calculation capability. One common fact is that they employ the same fine group width, namely 1/120 in lethargy to perform the slowing down calculation by taking into account the characteristic of the fast neutron spectrum. Another common fact is that the calculations are carried out based on their own pre-generated hyperfine group XS libraries which are processed through their own in-house XS manipulation codes which are not generally available.

The main purpose of this work is to provide highly reliable MG

XS data for fast reactor analyses with pin-level resolution through the direct whole core calculation code nTRACER by directly using the ENDF format nuclear data files. To meet the purpose, pointwise XS data need to be prepared first for the use in slowing down calculations. In the slowing down calculation, spatial modeling as well as detailed energy modeling should be considered in order to incorporate the heterogeneity effects. As a result of this work, a fast reactor MG XS generation code EXUS-F (Effective X-section generation code employing Ultrafine group transport Solution for Fast reactor analysis) was developed. As mentioned above, the ENDF format nuclear data libraries are updated once in a while and there are different kinds of nuclear data libraries. Also the ENDF format nuclear data processing system NJOY is publicly available. It would thus be beneficial to generate MG XSs with direct processing the ENDF format nuclear data libraries instead of using the pre-generated library.

To obtain the pointwise XSs from the ENDF format nuclear data files, the RECONR module of the NJOY system is introduced to reconstruct the pointwise XS using the resonance parameters. In the reconstruction of the pointwise XS, the Doppler broadening effect is also incorporated using the BROADR module of NJOY. The Doppler broadening calculation of the major heavy nuclides is performed by an internal module that uses the Gauss-Hermite quadrature instead of using the BROADR module of NJOY in order to save the excessive computing time required for calculations with thermal feedback. It is noted that the pointwise XS data in MC^2-3 is prepared based on the MC^2-3 library from the ETOE code[5] of ANL which produces the MC^2-3 library from the ENDF format nuclear data libraries. The resonance parameters in the nuclear data library are converted to the multipole data in ETOE to perform the resonance reconstruction and the Doppler broadening calculation simultaneously. However, the conversion of the resonance parameters essentially requires a pre-generated library and verifications of the converted data should be performed.

The slowing down calculations are performed in an ultrafine

group structure involving 2123 groups for the detailed energy modeling. The default lethargy width of 1/120 is the same as MC^2-3, but the upper energy limit is extended to 20 MeV instead of 14 MeV of Mc^2-3. However, the lethargy width and upper energy limit can be controlled by the user input and there is no limitation to extend the upper energy limit because all of threshold reactions are considered. Since *(n,3n)* reactions are important at the energy level above 14 MeV, the *(n,3n)* reaction is incorporated in EXUS while it is neglected in MC^2-3. Note that the nuclear data is given up to 20 MeV – 30 MeV in the recent ENDF files.

The ultrafine group width is still wider than the resonance widths of most heavy nuclides so that self-shielding should be considered in the UFG XS preparation. For the resolved resonance and above resonance range, the numerical integration scheme based on Doppler broadened pointwise XSs can be applied in the same way as MC^2-3. The subgroup method which has a great advantage of easy application to complex geometry problems was avoided here because it requires pre-generated subgroup parameters. For the unresolved resonance treatment, the probability table method is adopted in EUXS-F unlike MC^2-3. The PURR routine of NJOY is used to generate the probability tables. Note that the probability table contains probability data as a function of energy instead of UFG, thus it can be easily utilized for different group structures just by interpolating data.

The scattering matrices for higher order moments are obtained up to the user specified order. Not only elastic scattering, but also inelastic scattering and *(n,xn)* reactions are included by directly utilizing the angular (File 4), energy (File 5) and energy – angle (File 6) distribution data of the ENDF format data. Note that the scattering order of MC^2-3 is one for inelastic scattering and anisotropy is neglected for *(n,2n)* reactions. The fission matrix for each fissionable isotope is also determined from the energy distribution data.

For the slowing down calculation, consistent P_1 transport equation is solved for 0D mixture problems. In order to obtain the

higher order moments of the flux spectrum in the 0D problems that are required to incorporate the anisotropic scattering effect with the higher order moments of the MG scattering transfer matrix, the extended transport approximation is applied as in MC^2-3. In order to handle the local heterogeneity effect on MG XSs, the collision probability method (CPM) is incorporated for the 1D cylindrical geometry while the method of method of characteristics (MOC) is employed to the 2D hexagonal geometry.

This thesis consists of 5 parts. First, the methods to process the resonance data in the evaluated nuclear data files are presented in Chapter 2. Then, the methods needed for calculating the UFG XS and transfer matrices are described in Chapter 3 which include the generation of self-shielded XSs, fission and scattering transfer matrices from the evaluated nuclear data files. The transport calculation methods employed in EXUS-F are then presented in Chapter 4. The accuracy of the MG XS generator is verified in Chapter 5 with various geometry applications spanning from 0D problems to 2D core problems. Finally, the conclusion is given in Chapter 6.

Chapter 2. Resonance Data Processing

2.1. NJOY Based XS Reconstruction and Doppler Broadening

In the evaluated nuclear data files, the XSs are given pointwise in File 3 of the ENDF format only for limited energy ranges. One is the lower energy range (LER) where the Doppler effects can be negligible. The other is the high energy range (HER), where resonances are fully overlapped and the cross sections have a smooth shape. Except LER and HER, resonance parameters are given in File 2 of the ENDF format for individual resonances in different resonance models such as single-level Breit-Wigner (SLBW), multi-level Breit-Wigner (MLBW), Reich-Moore, etc. Sometimes, the XSs in the LER are omitted and given as the resonance parameters. For example, the resolved resonance range of ^{235}U is from 1.e-5 eV to 2.25 keV in the ENDF/B-VII library. It means that if the reconstruction is not performed, the data as shown in Figure 2-2 can't be obtained and only the data such in the Figure 2-1 is obtained.

In order to reconstruct pointwise XSs from given resonance models and parameters, the NJOY routines[9] are utilized instead of realizing its own reconstruction capability. Specifically, if there is no pre-saved pointwise XS file in the local folder, for a nuclide at a temperature of interest, EUXS-F checks the existence of the corresponding pointwise XS file at 0 K. If it exists, the Doppler broadening calculation is performed based on the pointwise XS at 0 K by using the internal functions of EXUS-F, which will be discussed in the next section. If there is no data at 0 K, EXUS-F invokes the NJOY code after writing an input file for the RECONR and BROADR modules of NJOY. The resulting pointwise XS data at specified temperatures are stored in a binary file for a later use, since the run time of the RECONR module is considerable long.

Figure 2-3 represents the process to prepare the Doppler broadened pointwise XS using NJOY.

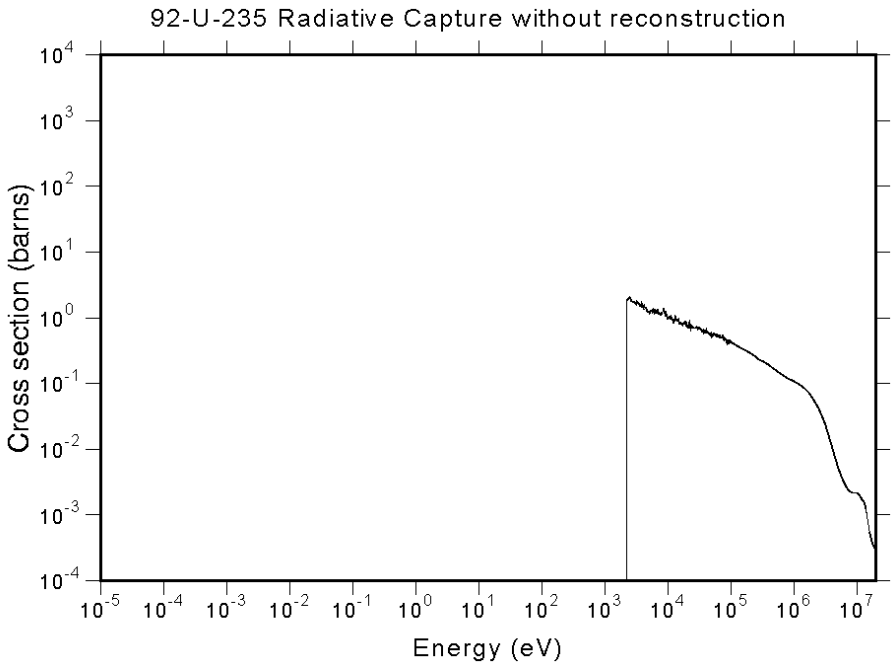

Figure 2-1. Capture XSs of U-235 before Resonance Data Reconstruction

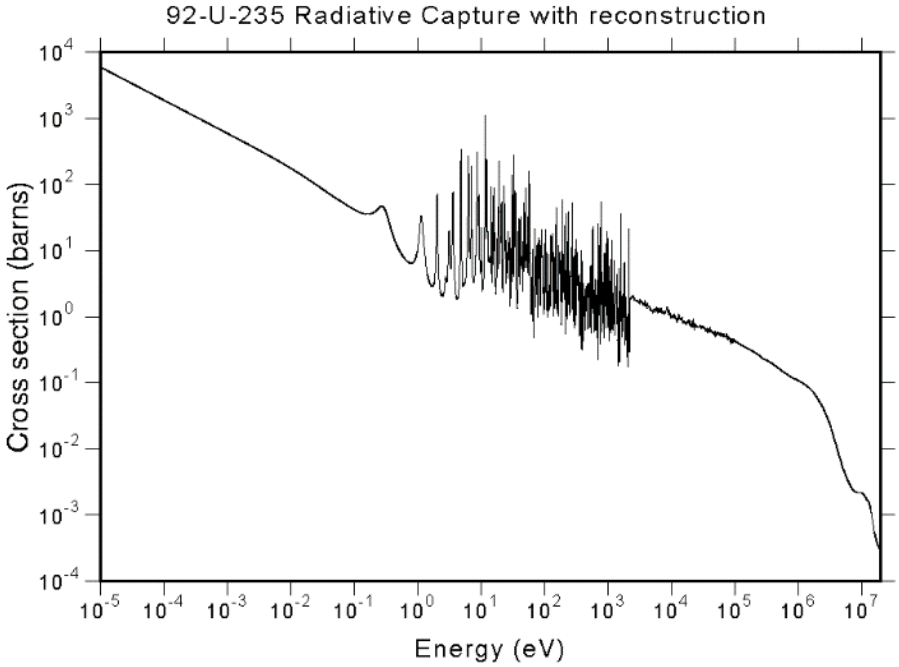

Figure 2-2. Capture XSs of U-235 after Resonance Data Reconstruction

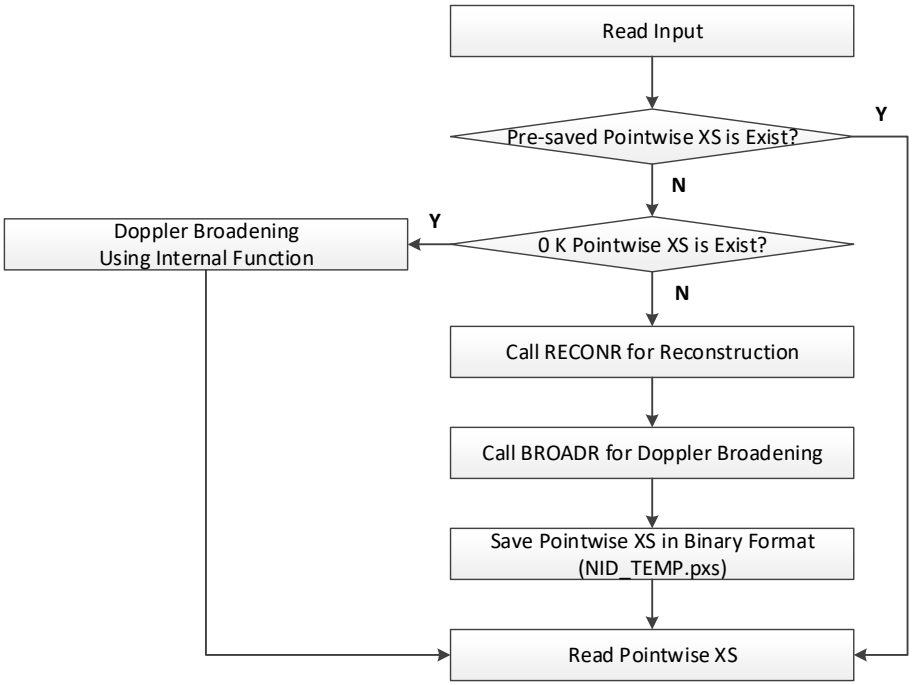

Figure 2-3. Flow Chart of EXUS-F for Reconstruction and Doppler Broadening of Resonances by NJOY

2.2. On-the-fly Doppler Broadening

As mentioned above, the Doppler broadening calculation is performed with the BROADR module of NJOY. The BROADR module requires the reconstructed pointwise XSs in the PENDF format. However, the PENDF file includes additional data and thus its size is more than ten times larger than the binary pointwise XS file of EXUS-F. the pointwise XS reconstruction with the RECONR module also requires considerable computation times, especially for heavy nuclides. To reduce the computation time and memory requirement, two on-the-fly Doppler broadening methods are incorporated in EXUS-F.

2.2.1. SIGMA1 Method

The SIGMA1 method was originally developed by D. E. Cullen[15] and it is invoked in the BROADR module of NJOY. It uses a detailed integration of the integral equation defining the effective cross section, thus it gives accurate results.

The Doppler broadened cross section at a temperature T can be expressed as:

$$\bar{\sigma}(v,T) = \frac{1}{v^2}\sqrt{\frac{\alpha}{\pi}}\int_0^\infty \sigma(v_r) v_r^2 \left\{ e^{-\alpha(v_r - v)^2} - e^{-\alpha(v_r + v)^2} \right\} dV \qquad (2.1)$$

where, $\alpha = M / 2kT$, M is the atomic mass of the target nuclide, k is the Boltzmann constant, v is the neutron velocity corresponding the neutron incident energy E *and* v_r is the relative speed of between the target and the incident neutron. Eq. (2.1) can be divided into two parts as:

$$\bar{\sigma}(v,T) = \sigma^*(v,T) - \sigma^*(-v,T) \qquad (2.2)$$

with a function

$$\sigma^*(v,T)=\frac{1}{v^2}\sqrt{\frac{\alpha}{\pi}}\int_0^\infty \sigma(v_r)v_r^2 e^{-\alpha(v_r-v)^2}dv_r\,. \tag{2.3}$$

The Gaussian function in Eq. (2.3) has a standard deviation $\sigma=1/\sqrt{\alpha}$, thus the function limits the significant part of the integral to the range within 4σ

$$v-\frac{4}{\sqrt{\alpha}}<v_r<v+\frac{4}{\sqrt{\alpha}}\,. \tag{2.4}$$

For $\sigma^*(-v,T)$, the integral depends only on velocities in the range

$$0<v_r<\frac{4}{\alpha}. \tag{2.5}$$

For the numerical integration of Eq. (2.3), the cross section in the integrand is assumed as a function of energy between two given energy points. If the cross section can be represented by a piecewise linear function of energy, the cross section can be expressed as:

$$\sigma(x)=\sigma_i+s_i(x^2-x_i^2) \tag{2.6}$$

where, σ_i is a cross section at an energy point *i*, s_i is a slope defined as $\sigma_i=(\sigma_{i+1}-\sigma_i)/(x_{i+1}^2-x_i^2)$, and $x_i=\sqrt{\alpha}v_r$.

With Eq. (2.6), Eq. (2.3) can be rewritten as:

$$\sigma^*(y,T)=\frac{1}{\sqrt{\pi}y^2}\sum_i\int_{x_i}^{x_{i+1}}\sigma(x)x^2e^{-(x-y)^2}dx \tag{2.7}$$

where $y=\sqrt{\alpha}v$. Eq. (2.7) can be solved analytically based on the incomplete probability integrals.

$$\sigma^*(y,T) = \sum_i \left[A_i(\sigma_i - s_i x_i^2) + B_i s_i \right]$$

$$\text{where} \quad A_i = \frac{1}{y^2} H_2 + \frac{2}{y} H_1 + H_0, \text{ and} \tag{2.8}$$

$$B_i = \frac{1}{y^2} H_4 + \frac{4}{y} H_3 + 6H_2 + 4yH_1 + y^2 H_0$$

The function H_n in above stands for $H_n(x_i - y, x_{i+1} - y)$ and it can be computed by using a recursion relation of a function $F_n(a)$ which is described below.

$$\begin{aligned} H_n(a,b) &= \frac{1}{\sqrt{\pi}} \int_a^b z^n e^{-z^2} dz \\ &= F_n(a) - F_n(b) \end{aligned} \tag{2.9}$$

The function F_n satisfy a recursion relation as below.

$$F_n(a) = \frac{1}{\sqrt{\pi}} \int_a^\infty z^n e^{-z^2} dz \tag{2.10}$$

$$F_0(a) = \frac{1}{2} erfc(a) \tag{2.11}$$

$$F_1(a) = \frac{1}{2\sqrt{\pi}} \exp(-a^2) \tag{2.12}$$

$$F_n(a) = \frac{n-1}{2} F_{n-2}(a) + a^{n-1} F_1(a) \tag{2.13}$$

2.2.2. Gauss-Hermite Quadrature Method

The other way to calculate the Doppler broadening effect on-the-fly is use of the Gauss-Hermite quadrature for the integration in Eq. (2.1)[16]. By applying the Gauss-Hermite quadrature, the Doppler broadened XS at a temperature T can be obtained using the formula:

$$\begin{aligned}\sigma(v,T) &= \frac{1}{v^2}\sqrt{\frac{\alpha}{\pi}}\int_0^\infty \left\{e^{-\alpha(v-v_r)^2} - e^{-\alpha(v+v_r)^2}\right\} v_2{}^2\sigma(v_r,T_1)dv_r \\ &= \frac{1}{v^2}\sqrt{\frac{\alpha}{\pi}}\int_{-\infty}^\infty \mathrm{sgn}(v_r)e^{-\alpha(v-v_r)^2} v_r{}^2\sigma\left(|v_r|,T_1\right)dv_r\end{aligned} \tag{2.14}$$

where T_1 is a temperature for the base XS and $\mathrm{sgn}(x)$ is the sign function.

The quadrature order for the Gauss-Hermite quadrature method was determined based on numerical tests.

Figure 2-4 and Figure 2-5 show RMS differences of the Doppler broadened total XSs of 5 important isotopes in the fast reactor analysis. It can be seen that 9 is enough as the quadrature order for the Doppler broadening calculation.

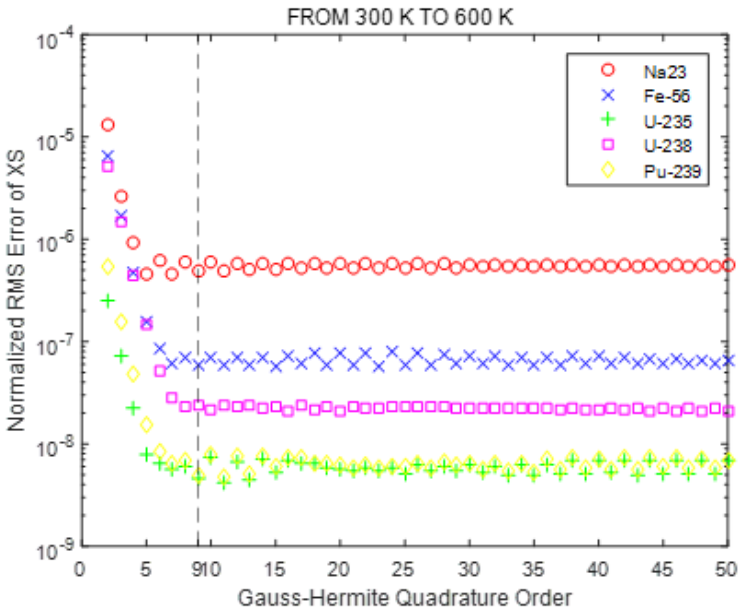

Figure 2-4. RMS. Differences of Doppler Broadened XSs at 600 K based on the XSs at 300 K using the Gauss-Hermite Method (References: BROADR)

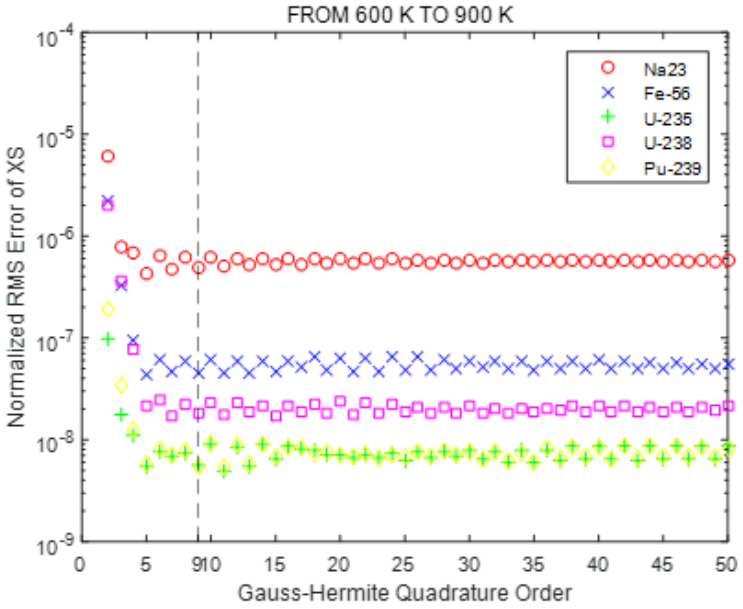

Figure 2-5. RMS. Differences of Doppler Broadened XSs at 900 K based on the XSs at 600 K using the Gauss-Hermite Method (References: BROADR)

2.2.3. Doppler Broadening Procedure in EXUS-F

The SIGMA1 method gives accurate values by solving the

integral with all of energy points within the integration range, thus it is slow. On the other hand, the Gauss-Hermite quadrature method is faster but has limited applications. Because the Gauss-Hermite quadrature does not approximate well a function with drastic changes, it cannot be used for broadening from 0 K or for intermediate mass nuclides that have very narrow resonances such as Fe-56, as shown in Figure 2-6. Lines at 0.1% in the figure means the tolerance for linear representation of the XS.

To examine a validity of the Gauss-Hermite quadrature method, simple numerical test was carried out. For all isotopes in the ENDF/B-VII.0 library, the Doppler broadened XSs at 600 K were calculated using the SIGMA1 method using 0 K base XSs and the Gauss-Hermite quadrature method using 300 K base XSs. And the XSs were compared with reference XSs from the BROADR module of NJOY. The result of the numerical test is presented in Figure 2-7. As shown in the Figure, the SIGMA1 method always show good performances, but errors larger than 0.1 % tolerance are observed in intermediate mass isotopes. However, the Gauss-Hermite method give acceptable results for heavy nuclides. And the average computing times for the Doppler broadening calculation, ~0.045 sec for heavy nuclides is about 20 times faster than the SIGMA1 method, ~1.023 sec.

Based on these results of the numerical test, the Gauss-Hermite quadrature method is used only for broadening of heavy nuclides XSs from non-zero temperature. The SIGMA1 method covers other cases. Figure 2-8 represents the process to perform the Doppler broadening calculation based on the pre-saved XS in EXUS-F.

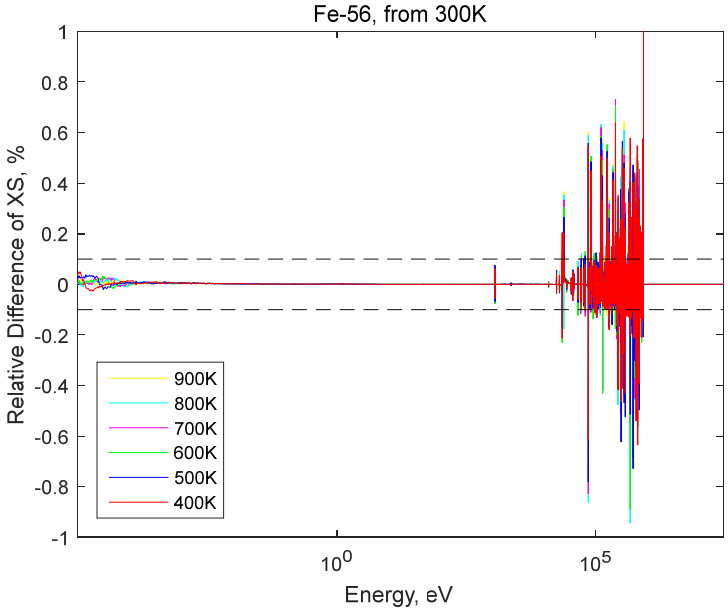

Figure 2-6. Relative Differences of Fe-56 Total XS between the Gauss-Hermite Quadrature Method and BROADR

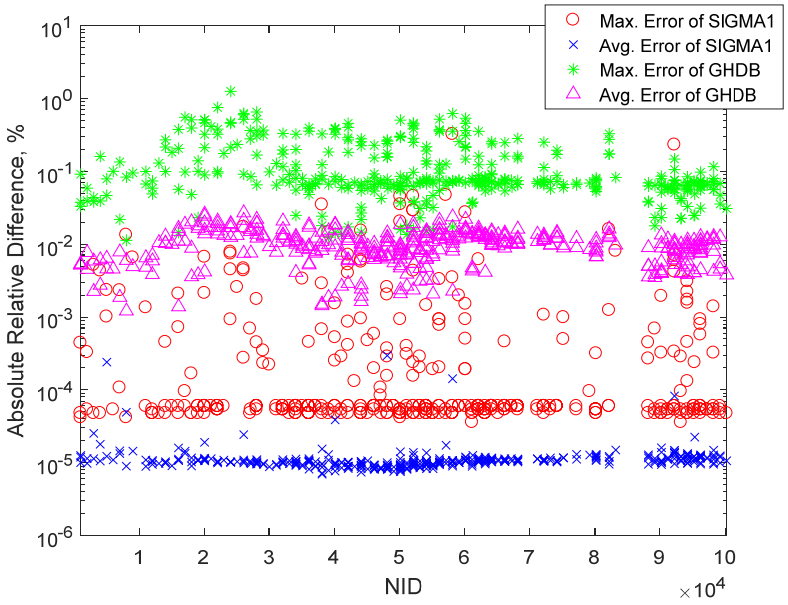

Figure 2-7. Max. and RMS. Differences of Total XSs for all isotopes in ENDF/B-VII.0 between the Gauss-Hermite Quadrature method and BROADR

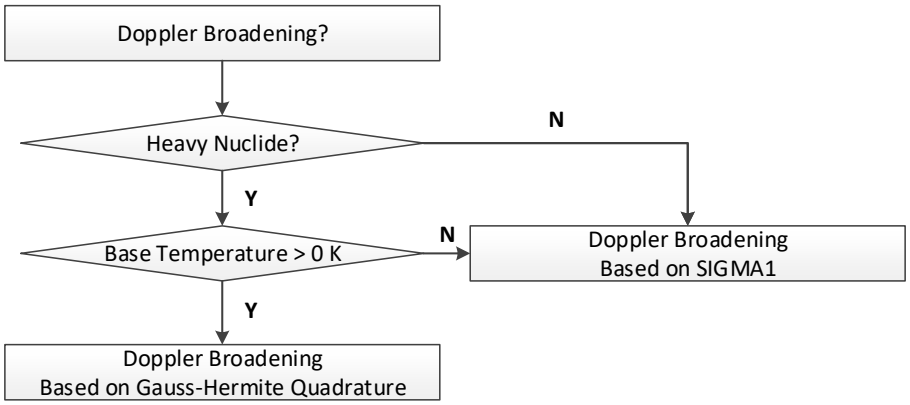

Figure 2-8. Flow Chart of EXUS-F for Doppler Broadening Calculations using Pre-generated XSs

2.3. Union Energy Grid

Doppler broadened XSs of different isotopes are calculated at different energy grids. Later, these cross sections are recalculated at a union energy grid by interpolation in order to determine the macroscopic total XSs of specified compositions, which are required for resonance self-shielding. To calculate the macroscopic total XSs, an adaptive energy grid is determined for each composition in such a way that each XS can be linearized in the energy grid within a user-specified tolerance with a default value of 0.1%. Instead of the adaptive energy grid, fixed energy grid can also be taken such as 200 points per an UFG.

Chapter 3. Generation of Ultrafine Group Cross Sections and Transfer Matrices

3.1. Energy Group Structures

EXUS-F uses an ultrafine energy group structure for transport calculations. The current ultrafine energy group structure consists of 2123 energy groups and the upper and lower energy bounds are 20 MeV and 0.413 eV, respectively. All the energy groups have the same lethargy width of 1/120 as MC^2-3. This lethargy width is corresponding to the average lethargy gain of U-238 and it means the most of the neutrons having a collision in an ultrafine group can escape from the energy group. Additionally, the user can specify the number of energy groups, the upper and lower energy bounds, and the UFG lethargy width.

3.2. Resonance Self-Shielding for Resolved Range and Above Resonance Ranges

3.2.1. Neutron Flux in the NR Approximation

The UFG width is still very wide relative to heavy isotope resonances, and thus the self-shielded XSs are determined for each UFG with the following definition:

$$\bar{\sigma}_{i,x,g} = \int_{\Delta u_g} \sigma_{x,i}(u)\phi(u)du \,/\, \int_{\Delta u_g} \phi(u)du \qquad (3.1)$$

where, i, x and g are the indices for isotope, reaction type and ultrafine energy group, respectibly. Using the narrow resonance (NR) approximation, the neutron spectrum in each composition can be approximated as

$$\phi(u) = \Sigma_p / (\Sigma_t(u)) . \qquad (3.2)$$

The NR approximation is valid when the resonance width is much narrower than the average energy loss per neutron scattering, thus it is valid in the most energy range higher than 100 eV. Inserting Eq. (3.2) into Eq. (3.1) yields

$$\bar{\sigma}_{x,i,g} = \int_{\Delta u_g} \frac{\sigma_{x,i}(u)}{\Sigma_t(u)} du \Big/ \int_{\Delta u_g} \frac{1}{\Sigma_t(u)} du . \qquad (3.3)$$

The integrations in Eq. (3.3) are evaluated with the Simpson's rule using the pointwise XSs interpolated at the adaptive energy grid or the fixed energy grid. Figure 3-1 shows pointwise total XS of Na-23 and its self-shielded XS with the UFG structure.

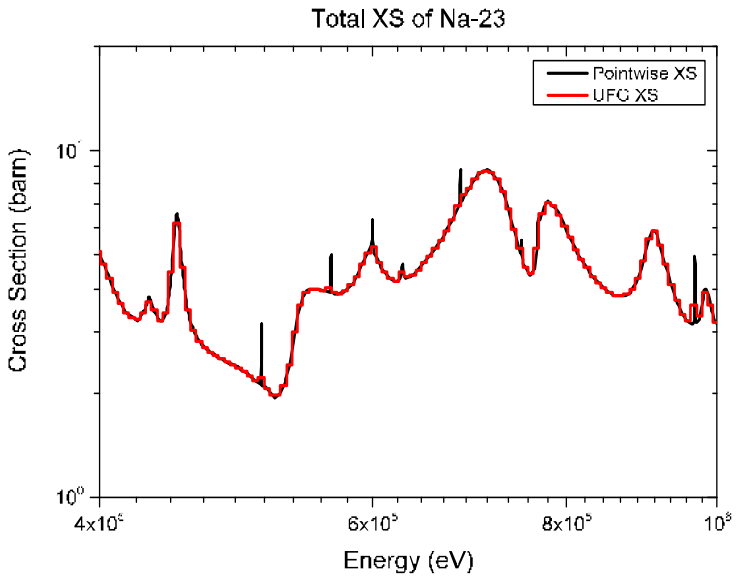

Figure 3-1. Pointwise and Self-shielded UFG Total XS of Na-23

3.2.2. Higher moment fluxes in the Bondarenko Model

The higher order angular moments of the neutron spectrum are required for self-shielding of anisotropic total XSs or scattering XSs. The moments can be determined with the B_0 approximation in large size core problem. [17]

The Boltzmann transport equation with isotropic fission source and without an external source can be written in terms of lethargy as:

$$\nabla \cdot \hat{\Omega}\varphi(\vec{r},u,\hat{\Omega}) + \Sigma_t(u)\varphi(\vec{r},u,\hat{\Omega}) = S_s(\vec{r},u,\hat{\Omega}) + \frac{1}{4\pi}S_f(\vec{r},u) \qquad (3.4)$$

where $\varphi(\vec{r},u,\hat{\Omega})$ is the neutron angular flux at location $\vec{r}$, lethargy u, and angle $\hat{\Omega}$, S_s is the scattering source and S_f is the isotropic fission source. If a homogenous mixture is assumed, then the angular flux $\varphi(\vec{r},u,\hat{\Omega})$ in Eq. (3.4) can be expressed as:

$$\varphi(\vec{r},u,\hat{\Omega}) = \varphi(\vec{r},u)e^{-iB\cdot\vec{r}} \qquad (3.5)$$

where B^2 is the buckling.

Insertion of Eq. (3.5) to Eq. (3.4) makes the Boltzmann transport equation to be represented as:

$$(iB\cdot\hat{\Omega} + \Sigma_t(u))\varphi(u,\hat{\Omega}) = \int_{u'}\int_{4\pi}\Sigma_s(u'\to u,\hat{\Omega}'\cdot\hat{\Omega})\varphi(u',\hat{\Omega}')d\hat{\Omega}'du' + \frac{1}{4\pi}S_f(u) \qquad (3.6)$$

Taking the coordinates such that the direction of B is the positive z axis, Eq. (3.6) can be rewritten as:

$$(iB\mu + \Sigma_t(u))\varphi(u,\hat{\Omega}) = \int_{u'}\int_{4\pi}\Sigma_s(u'\to u,\hat{\Omega}'\cdot\hat{\Omega})\varphi(u',\hat{\Omega}')d\hat{\Omega}'du' + \frac{1}{4\pi}S_f(u) \qquad (3.7)$$

where $\mu = \hat{\Omega}' \cdot \hat{\Omega}$ is the cosine of the scattering angle in the laboratory system.

If the neutron flux $\varphi(u, \hat{\Omega})$ is symmetry in the azimuthal angle, the scattering source in RHS of (3.7) can be reduced by Legendre expansion to:

$$S_s(u, \hat{\Omega}) = \sum_{l=0}^{\infty} \frac{2l+1}{4\pi} P_l(\mu) \int_{u'} \Sigma_{sl}(u' \to u) \phi_l(u') du' \tag{3.8}$$

where $P_l(\mu)$ is the l–th order Legendre polynomial. By inserting Eq. (3.8) and multiplying 2π in both sides, Eq. (3.6) can be represented as:

$$\begin{aligned}(iB\mu + \Sigma_t(u))\varphi(u, \mu) = & \sum_{l=0}^{\infty} \frac{2l+1}{2} P_l(\mu) \int_{u'} \Sigma_{sl}(u' \to u) \phi_l(u') du' \\ & + \frac{1}{2} S_f(u)\end{aligned} \quad . \tag{3.9}$$

Multiplying $P_n(\mu) / (1 + iB\mu / \Sigma_t)$ in both terms of Eq. (3.9) and integrating over μ gives

$$\begin{aligned}\Sigma_t \phi_n(u) = & \sum_{l=0}^{\infty} (2l+1) A_{nl}(u) \int_{u'} \Sigma_{sl}(u' \to u) \phi_l(u') du' \\ & + A_{n0}(u) S_f(u), \quad n = 0, 1, \cdots\end{aligned} \tag{3.10}$$

where

$$\begin{aligned}A_{nl}(u) &= \frac{1}{2} \int_{-1}^{+1} \frac{P_n(\mu) P_l(\mu)}{1 + iB\mu / \Sigma_t} d\mu \\ &= \frac{1}{2} \int_{-1}^{+1} \frac{P_n(\mu) P_l(\mu)}{1 - \mu / z(u)} d\mu, \quad z(u) = -\Sigma_t(u) / iB\end{aligned} \quad . \tag{3.11}$$

The coefficients A_{nl} for $l=0$ can be calculated by

$$\begin{aligned} A_{n0} &= \frac{1}{2}\int_{-1}^{+1}\frac{P_n(\mu)}{1-\mu/z}d\mu = \frac{z}{2}\int_{-1}^{+1}\frac{P_n(\mu)}{z-\mu}d\mu \\ &= zQ_n(z) = -\frac{\Sigma_t}{iB}Q_n(-\frac{\Sigma_t}{iB}) \end{aligned} \tag{3.12}$$

where Q_n is the Legendre function of the second kind that is the second solution of the Legendre differential equation. An integral representation of $Q_n(z)$ is given by

$$Q_n(z) = \frac{1}{2}\int_{-1}^{+1}\frac{P_n(t)}{z-t}dt = (-1)^{n+1}Q_n(-z). \tag{3.13}$$

The Legendre function of the second kind has the following recurrence relation.

$$(2n+1)zQ_n(z) = (n+1)Q_{n+1}(z) + nQ_{n-1}(z) \tag{3.14}$$

The recurrence relation for the coefficient A_{nl} can be obtained from the recurrence relation of the Legendre polynomial $P_l(\mu)$.

$$(2l+1)zA_{nl}(z) = (l+1)A_{n,l+1}(z) + lA_{n,l-1}(z) + z\delta_{nl} \tag{3.15}$$

Additionally, the coefficient A_{nl} is symmetric, i.e., $A_{nl} = A_{ln}$, thus the coefficient A_{nl} can be calculated by using these properties and A_{n0} in (3.12).

In B_N approximation, it is assumed that

$$\int_{u'}\Sigma_{sn}(u' \to u)\phi_n(u')du' = 0, \quad n > N. \tag{3.16}$$

Thus, Eq. (3.10) becomes

$$\Sigma_t \phi_n(u) = \sum_{l=0}^{\infty} (2l+1) A_{nl}(u) \int_{u'} \Sigma_{sl}(u' \to u) \phi_l(u') du' + A_{n0}(u) S_f(u), \qquad n = 0,1,\cdots N \quad . \tag{3.17}$$

This is a set of coupled equation for the B_N approximation.

For $n > N$, Eq. (3.9) can be rewritten by multiplying $P_n(\mu)$ and integrating over μ as

$$(2n+1)\left(-\frac{\Sigma_t}{iB}\right)\phi_n(u) = (n+1)\phi_{n+1}(u) + n\phi_{n-1}(u), \quad n > N \, . \tag{3.18}$$

This shows that ϕ_n satisfies the similar recurrence relation as $Q_n(z)$ in Eq. (3.14), where $z = -\Sigma_t / iB$. Thus, the solution of Eq. (3.18) can be assumed as

$$\phi_n(u) = c(u) Q_n(-\Sigma_t(u) / iB), \qquad n > N \, . \tag{3.19}$$

Thus, the approximation in Eq. (3.16) is equivalent to

$$\phi_n(u) = \phi_N(u) \frac{Q_n(-\Sigma_t(u) / iB)}{Q_N(-\Sigma_t(u) / iB)}, \quad n > N \, . \tag{3.20}$$

If the scattering source is almost isotropic, the higher flux moments are determined by

$$\phi_n(u) = \frac{Q_n(-\Sigma_t(u) / iB)}{Q_0(-\Sigma_t(u) / iB)} \phi_0(u), \quad n = 1,2,\cdots . \tag{3.21}$$

On the other hand, the Legendre functions of the second kind can be represented by infinite series.

$$Q_n(x) = \frac{2 \times (n!)^2}{(2n+1)!} \left[\left(\frac{1}{x}\right)^{n+1} + \frac{(n+1)(n+2)}{2(n+3)} \left(\frac{1}{x}\right)^{n+3} + C_3 \left(\frac{1}{x}\right)^{n+5} + \cdots \right] \tag{3.22}$$

If the domain size is large enough, $|B|/\Sigma_t \ll 1$, Eq. (3.22) is approximated as

$$Q_n(x) \approx \frac{2(n!)^2}{(2n+1)!}\left(\frac{1}{x}\right)^{n+1}. \tag{3.23}$$

With Eq. (3.23), Eq. (3.21) is reduce to

$$\phi_n(u) \approx \frac{(n!)^2(-iB)^n}{(2n+1)!}\left(\frac{1}{\Sigma_t(u)}\right)^n \phi_0(u), \qquad n=1,2,\cdots. \tag{3.24}$$

Finally, higher moment fluxes can be obtained from Eq. (3.24) with the NR approximation as below:

$$\phi_n(u) = a \cdot \frac{(-i)^n}{\Sigma_t(u)^{n+1}} \tag{3.25}$$

where a is a coefficient.

With Eq. (3.25), n-th order UFG self-shielded reaction XS can be obtained as

$$\sigma_{x,n,g} = \frac{\int_{\Delta u_g} \frac{\sigma_x(u)}{(\Sigma_t(u))^{n+1}} du}{\int_{\Delta u_g} \frac{1}{(\Sigma_t(u))^{n+1}} du}. \tag{3.26}$$

3.3. Self-Shielding for Unresolved Resonance Range

In the unresolved resonance energy range (URR), the experimental resolution is larger than the width of the resonances and hence individual resonance can no longer be parameterized deterministically. In the evaluate nuclear data files, therefore, average values are provided for the level spacing and partial widths along with the corresponding probability distributions. However, the resonance self-shielding in URR is important especially in fast reactor applications[18].

The cross sections in the unresolved resonance range are self-shielded using the probability table method. For this, a library of probability tables should be prepared using the PURR module of NJOY based on the evaluated nuclear data libraries such as ENDF/B-VII.0, ENDF/B-VII.1 and JENDL 4.0. Each probability table is computed in 20 probability bins at 7 temperatures from 0 K to 3000 K with a uniform interval of 500 K using 64 ladders. In the case of the ENDF/B-VII.0 library includes the probability table for all 253 nuclides with unresolved resonance parameters and its size is about 20 MB.

Under the approximation that the UFG width is so fine that the probability and cross section values and the background cross sections are constant within each group, the self-shielded XS in Eq. (3.3) can be evaluated using the probability table data as:

$$\bar{\sigma}_{x,i,g} = \frac{\sum_k \frac{P_{i,g}^k \sigma_{x,i,g}^k}{N_i(\sigma_{t,i,g}^k + \sigma_{0,i,g})}}{\sum_k \frac{P_{i,g}^k}{N_i(\sigma_{t,i,g}^k + \sigma_{0,i,g})}} \tag{3.27}$$

where, $P_{i,g}^k$ and $\sigma_{x,i,g}^k$ are the probability and reaction XS values at the mid-point of each ultrafine group g for a probability bin k and $\sigma_{0,i,g}$ is the group-averaged background XS for isotope i.

$$\sigma_{0,i,g} = \frac{1}{N_i} \sum_{j \neq i} N_j \bar{\sigma}_{t,i,g} \ . \tag{3.28}$$

In the group where the boundary between resolved and unresolved resonance ranges located, both resolved and unresolved resonances are self-shielded simultaneously. By dividing the integration range into the resolved and unresolved resonance intervals, the self-shielded XS is determined as

$$\bar{\sigma}_{i,x,g} = \frac{\int_{\Delta u_{resolved}} \sigma_{x,i}(u)\phi(u)du + \int_{\Delta u_{unresolved}} \sigma_{x,i}(u)\phi(u)du}{\int_{\Delta u_{resolved}} \phi(u)du + \int_{\Delta u_{unresolved}} \phi(u)du} \tag{3.29}$$

where the integrals over the resolved resonance interval are evaluated as in Eq. (3.3) and the integrals over the unresolved resonance interval are evaluated as in Eq. (3.27). The final form of the self-shielded XS in the boundary group is expressed as

$$\bar{\sigma}_{i,x,g} = \frac{\int_{\Delta u_{resolved}} \sigma_{x,i}(u)\phi(u)du + \Delta u_{unresolved} \sum_k \frac{P_{i,g}^k \sigma_{x,i,g}^k}{N_i(\sigma_{t,i,g}^k + \sigma_{0,i,g})}}{\int_{\Delta u_{resolved}} \phi(u)du + \Delta u_{unresolved} \sum_k \frac{P_{i,g}^k}{N_i(\sigma_{t,i,g}^k + \sigma_{0,i,g})}}. \tag{3.30}$$

Figure 3-2 shows the pointwise and self-shielded group values of U-238 total XS at the boundary group between the resolved resonance and unresolved resonance ranges.

In the preparation of self-shielded XSs, the probability table at a specified temperature is determined by interpolating the probability tables in the library prepared at seven temperatures. The interpolation is performed under the assumption that XSs are inversely proportional to the absolute temperature. Eq. (3.31) represents the temperature interpolation rule for the probability table at a temperature T between temperature T_1 and T_2.

$$x_i^k(T) = \frac{\log(T_2/T)}{\log(T_2/T_1)} x_i^k(T_1) + \frac{\log(T/T_1)}{\log(T_2/T_1)} x_i^k(T_2) \qquad (3.31)$$

where x_i^k is a probability $P_{i,g}^k$ or cross section $\sigma_{x,i,g}^k$ in the corresponding probability table.

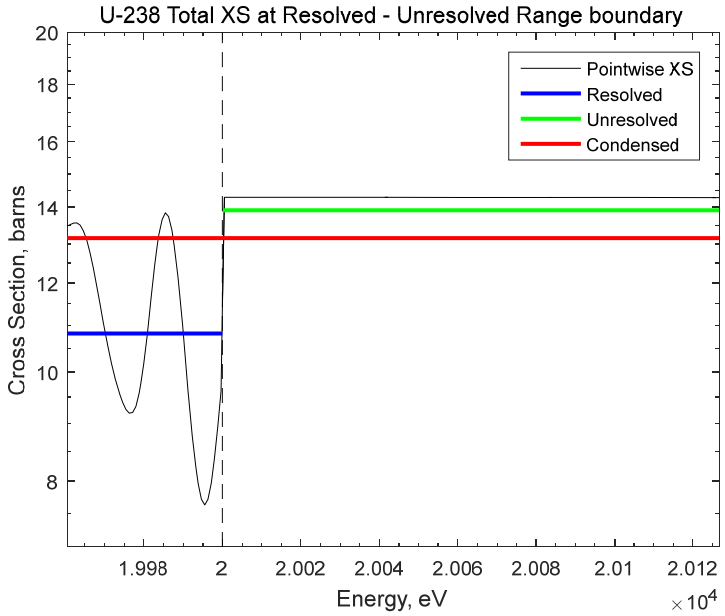

Figure 3-2. Pointwise and Condensed Values of U-238 Total XS at the Boundary of Resolved and Unresolved Resonance Ranges

3.4. Fission Spectrum Matrix

The fission spectrum is a distribution of fission neutrons' energies after fission reactions. The fission spectrum depends on the incident neutron energy, so it is often represented as the fission spectrum matrix in the multigroup structure. It can be calculated based on the energy distribution in File 5 of the evaluated nuclear data files using the fission spectrum vector depending on the incident neutron energy. The MG fission spectrum vector is defined as:

$$\begin{aligned}\chi_{i,g\to g'} &= \int_{\Delta E_g} \chi_{i,g'}(E)dE \\ &= \int_{\Delta E_g} \frac{\int_{\Delta E_{g'}} \chi_i(E,E')dE'}{\int_{E_{\min}}^{E_{\max}} \chi_i(E,E')dE'} dE\end{aligned} \tag{3.32}$$

where, i is an index for isotope, g and g' are an indices for incident and outgoing energy group, E is the incident neutron energy and E' is the outgoing neutron energy after fission. The angular distribution of fission neutrons is assumed isotropic.

The fission spectrum matrix can be calculated based on the energy distribution in File 5 of the evaluated nuclear data files. Table 3-1 shows data formats of the fission spectrum matrix for 62 fissionable nuclides in the ENDF/B-VII.0 library.

Table 3-1. Data Formats for Fission Spectrum Matrix in ENDF/B-VII.0

Format	Number of Data
Arbitrary Tabulated Function	10
Simple Maxwellian Fission Spectrum	49
Energy-Dependent Watt Spectrum	1
Madland-Nix Spectrum	2

3.4.1. Arbitrary Tabulated Function

The fission energy transfer function $\chi(E \rightarrow E')$ is directly given as tabulated values with incident and outgoing neutron energies. In this case, the fission spectrum matrix in Eq. (3.32) can be calculated analytically using given interpolation laws for incident and outgoing energies.

3.4.2. Simple Maxwellian Fission Spectrum

The energy distribution in this format is given with a constant U and $\theta(E')$ as a function of incident neutron energy E. Based on the tabulated parameters, the fission energy transfer function is expressed as:

$$\chi(E,E') = \frac{\sqrt{E'}}{I} e^{-E'/\theta(E)}. \tag{3.33}$$

I in Eq. (3.33) is a normalization constant and defined as below. U is a constant to define the upper energy limit of the secondary particle. The energy range for secondary particle is determined as $0 \le E' \le (E-U)$.

$$I = \theta^{3/2}\left[\frac{\sqrt{\pi}}{2} erf\left(\sqrt{(E-U)/\theta} - \sqrt{(E-U)/\theta} e^{-(E-U)/\theta}\right)\right] \tag{3.34}$$

3.4.3. Energy-Dependent Watt Spectrum

In this format, coefficients a and b are provided as functions of energy with the constant U. The fission energy transfer function $\chi(E,E')$ is defined as:

$$\chi(E,E') = \frac{e^{-E'/a}}{I} \sinh(\sqrt{bE'}) \tag{3.35}$$

where i is a constant for normalization.

$$I=\frac{1}{2}\sqrt{\frac{\pi a^3 b}{44}}\exp(\frac{ab}{4})\left[erf\left(\sqrt{\frac{E-U}{a}}-\sqrt{\frac{ab}{4}}\right)\right]+erf\left(\sqrt{\frac{E-U}{a}}+\sqrt{\frac{ab}{4}}\right) \\ -a\exp\left[-\left(\frac{E-U}{a}\right)\right]\sinh\sqrt{b(E-U)} \tag{3.36}$$

3.4.4. Energy-Dependent Fission Neutron Spectrum (Madland and Nix)

In this format two constants $E_F(L)$, $E_F(H)$ and tabulated values $T_M(E)$ are given. With these values, the fission energy transfer function is defined as:

$$\chi(E,E')=\frac{1}{2}\left[g(E',E_F(L))+g(E',E_F(H))\right] \tag{3.37}$$

where,

$$g(E',E_F)=\frac{1}{3\sqrt{(E_F T_M}}\left[u_2^{3/2}E_1(u_2)-u_1^{3/2}E_1(u_1)+\gamma\left(\frac{3}{2},u_2\right)-\gamma\left(\frac{3}{2},u_1\right)\right] \\ u_1=\left(\sqrt{E'}-\sqrt{E_F}\right)^2/T_M \\ u_2=\left(\sqrt{E'}+\sqrt{E_F}\right)^2/T_M \tag{3.38}$$

and $\gamma(a,x)$ is the incomplete gamma function.

3.5. Scattering Transfer Matrix

EXUS-F calculates the scattering matrix for the neutron induced scattering reactions such as elastic scattering, discrete inelastic, and continuum inelastic scattering. The scattering matrix is also calculated for (n,2n) and (n,3n) reactions, including anisotropy, using the ENDF formatted nuclear data library.

An element of the scattering transfer matrix for the *l*-th anisotropic scattering can be represented as:

$$\sigma_{i,l,g\to g'} = \frac{\int_{E_g}^{E_{g-1}} \int_{E_{g'}}^{E_{g'-1}} \int_{-1}^{+1} \sigma_s(E)\phi_l(E) f(E \to E', \mu_s) P_l(\mu_s) d\mu_s dE' dE}{\int_{E_{g'}}^{E_{g'-1}} \phi_l(E) dE} \qquad (3.39)$$

where, $f(E \to E', \mu)$ being the scattering transfer probability from the incident energy E to the outgoing energy E' and the cosine of scattering angle μ_s in the lab system. $\phi_l(E)$ is *l*-th moment of neutron flux and $P_l(\mu_s)$ is the *l*-th order Legendre polynomial. With a given scattering transfer probability, the element of the scattering transfer matrix in Eq. (3.39) can be determined by evaluating the integrals numerically. The scattering transfer probability can be determined in three ways according to data types given in the nuclear data files: (1) the angular distribution in File 4, (2) the angular distribution in File 4 and the energy distribution in File 5, and (3) the energy-angle distribution in File 6.

In the case of two-body scattering such as elastic and discrete inelastic scattering, the information for the scattering transfer probability is only given in File 4 of the evaluated nuclear data. If only the angular distribution $f(E, \mu_s)$ is given, the transfer probability can be represented as:

$$f(E \to E', \mu_s) = f(E, \mu_s)\delta\left[E', E'(E, \mu_s)\right] \qquad (3.40)$$

and thus the element of the matrix can be rewritten as:

$$\sigma_{i,l,g\to g'} = \frac{\int_{E_g}^{E_{g-1}} \int_{\mu_s^{\min}}^{\mu_s^{\max}} \sigma_s(E)\phi(E) f(E,\mu_s) P_l(\mu_s) d\mu_s dE}{\int_{E_g}^{E_{g-1}} \phi(E) dE} \tag{3.41}$$

where $\mu_s^{\min}$ and $\mu_s^{\max}$ are the cosine corresponding to the lower and upper energy boundaries of the secondary energy group *g*. If the information about the secondary neutron is given in the center of mass (CM) system, Eq. (3.41) is changed to:

$$\sigma_{i,l,g\to g'} = \frac{\int_{E_g}^{E_{g-1}} \int_{\mu_c^{\min}}^{\mu_c^{\max}} \sigma_s(E)\phi(E) f(E,\mu_c) P_l[\mu_s(\mu_c)] d\mu_c dE}{\int_{E_g}^{E_{g-1}} \phi(E) dE}. \tag{3.42}$$

In the second case, the angular distribution and the energy distribution are given separately. This case applies to the continuum inelastic scattering and (*n,xn*) reactions. For some isotopes, the information for the discrete inelastic scattering is also given in this rule. When the angular and energy distributions are given separately, the transfer probability can also be separated to the angle and energy terms as:

$$f(E\to E',\mu_s) = f(E,\mu_s) g(E\to E') \tag{3.43}$$

where $g(E\to E')$ is the energy distribution from incident energy E' to emitted energy E. As a result, the matrix element in Eq. (3.39) can be calculated as below.

$$\sigma_{i,l,g\to g'} = \frac{\int_{E_g}^{E_{g-1}} \sigma_s(E)\phi_l(E) \left[\int_{-1}^{+1} f(E,\mu_s) P_l(\mu_s) d\mu_s\right] \left[\int_{E_{g'}}^{E_{g'-1}} g(E\to E') dE'\right] dE}{\int_{E_{g'}}^{E_{g'-1}} \phi_l(E) dE} \tag{3.44}$$

If the angular distribution is given in the CM system, Eq. (3.44) is modified in the same manner as Eq. (3.42) from Eq.

(3.41). Note that the energy distribution in File 5 is always given in the LAB system.

In the last case, the transfer probability $f(E \to E, \mu_s)$ is provided directly in File 6 as values or parameters. Therefore, the scattering matrix element can be calculated directly using Eq. (3.39) if the data is given in the LAB system. If the data is given in the CM system, i.e., the secondary energy E_c' and the cosine μ_c in the CM system, the transfer probability needs to be converted to the LAB system. Thus, the integration of a numerator in Eq. (3.39) is performed along the contour lines $E = constant$ using the Jacobian matrix.

$$J(E', \mu_c) = \sqrt{E' / E_c'} \tag{3.45}$$

As a result, the element can be expressed as:

$$\sigma_{i,l,g \to g'} = \frac{\int_{E_g}^{E_{g-1}} \int_{E_{g'}}^{E_{g'-1}} \int_{-1}^{+1} \sigma_s(E) \phi_l(E) f[E \to E_c'(E, E', \mu_s), \mu_c(E, E', \mu_s)] J(E', \mu_s) P_l(\mu_s) d\mu_s dE' dE}{\int_{E_{g'}}^{E_{g'-1}} \phi_l(E) dE}. \tag{3.46}$$

The denominator of the scattering transfer element is calculated numerically using the Simpson's rule, but the numerator is evaluated using the Gaussian quadrature with different quadrature orders. A quadrature order of five is for the integrations over the secondary energy and the cosine of the scattering angle. On the other hand, an order 32 is used for the integration over the incident energy to represent the variations of scattering XS and neutron flux within UFGs.

Optionally, the scattering matrix can be calculated with the assumption that the scattering reaction rate within a group is very smooth, as MC^2-3 does. With the approximation, Eq. (3.39) can be simplified as:

$$\sigma_{i,l,g'\to g} = \frac{\sigma_{s,l,g'}\phi_{l,g'}\int_{E_{g'}}^{E_{g'-1}}\int_{E_g}^{E_{g-1}}\int_{-1}^{+1} f(E'\to E,\mu_s)P_l(\mu_s)d\mu_s dE dE'}{\int_{E_{g'}}^{E_{g'-1}}\phi_l(E')dE'} \quad . \qquad (3.47)$$

$$= \sigma_{s,l,g'}\int_{E_{g'}}^{E_{g'-1}}\int_{E_g}^{E_{g-1}}\int_{-1}^{+1} f(E'\to E,\mu_s)P_l(\mu_s)d\mu_s dE dE'$$

Chapter 4. Ultrafine Group Transport Calculation

4.1. P_1 Slowing-Down Calculation with Extended Transport Approximation

The consistent P_1 transport equation is solved for homogeneous mixture problems in EXUS-F. The calculation is performed for each material and provides the UFG neutron flux spectrum to condense UFG XSs to a broad group structure. The critical buckling search option is available to determine the fundamental mode spectrum. For non-fuel assembly, the fission spectrum of a user-defined nuclide such as U-238 and Pu-239 can be utilized as a fission source.

4.1.1. Consistent P_n Equation

The Boltzmann transport equation in a homogenous mixture with the isotropic fission source and azimuthal symmetry of neutron angular flux is given in Eq. (3.9).

$$(iB\mu+\Sigma_t(u))\varphi(u,\mu)=\sum_{l=0}^{\infty}\frac{2l+1}{2}P_l(\mu)\int_{u'}\Sigma_{sl}(u'\to u)\phi_l(u')du' +\frac{1}{2}S_f(u) \tag{4.1}$$

By multiplying $P_n(\mu)$ and integrating over μ in both terms, above equation can be expressed as:

$$\int_{-1}^{+1}(iB\mu+\Sigma_t(u))\phi(u,\mu)P_n(\mu)d\mu=\int_{u'}\Sigma_{sn}(u'\to u)\phi_n(u')du' +\frac{1}{2}S_f(u)\delta_{n0},\quad n=0,1,2,\cdots \tag{4.2}$$

The angular flux $\varphi(u,\mu)$ in Eq. (4.2) can also be replaced using the spherical harmonics expansion.

$$\phi(u,\mu)=\sum_{l=0}^{\infty}\frac{2l+1}{2}\phi_l(u)P_l(u) \tag{4.3}$$

By inserting Eq. (4.3) into Eq. (4.2) and using the recursion relation of the Legendre polynomial, the consistent P_n equation can be obtained as follow.

$$\begin{aligned}&\frac{n+1}{2n+1}iB\phi_{n+1}(u)+\frac{n}{2n+1}iB\phi_{n-1}(u)+\Sigma_t(u)\phi_n(u)\\&\quad=\int_{u'}\Sigma_{sn}(u'\to u)\phi_n(u')du'+\frac{1}{2}S_f(u)\delta_{n0},\quad n=0,1,2,\cdots\end{aligned} \tag{4.4}$$

where $\phi_{-1}(u)=0$. It is assumed that $\phi_{N+1}(u)=0$ in P_n approximation, thus $N+1$ coupled equations are obtained from Eq. (4.4).

$$\begin{cases}iB\phi_1(u)+\Sigma_t(u)\phi_0(u)\\\qquad=\int\Sigma_{s0}(u'\to u)\phi_0(u')du'+\frac{1}{2}S_f(u), & n=0\\\frac{n+1}{2n+1}iB\phi_{n+1}(u)+\frac{n}{2n+1}iB\phi_{n-1}(u)+\Sigma_t(u)\phi_n(u)\\\qquad=\int\Sigma_{sn}(u'\to u)\phi_n(u')du', & n=1,2,\cdots,N-1\\\frac{N}{2N+1}iB\phi_{N-1}(u)+\Sigma_t(u)\phi_N(u)\\\qquad=\int\Sigma_{sN}(u'\to u)\phi_N(u')du', & n=N\end{cases} \tag{4.5}$$

By integrating Eq. (4.5) over group intervals, the consistent P_n multigroup equations can be written as:

$$\begin{cases} iB\phi_{1,g} + \Sigma_{t,g}\phi_{0,g} = \sum_{g'} \Sigma_{s0,g'\to g}\phi_{0,g'} + \frac{1}{2}S_{f,g}, & n=0 \\ \frac{n+1}{2n+1} iB\phi_{n+1,g} + \frac{n}{2n+1} iB\phi_{n-1,g} + \Sigma_{t,g}\phi_{n,g} & \\ \qquad = \sum_{g'} \Sigma_{sn,g'\to g}\phi_{n,g'}, & n=1,2,\cdots,N-1 \\ \frac{N}{2N+1} iB\phi_{N-1,g} + \Sigma_{t,g}\phi_{N,g} = \sum_{g'} \Sigma_{sN,g'\to g}\phi_{N,g'}, & n=N \end{cases} \tag{4.6}$$

4.1.2. Extended Transport Approximation

The angular flux moments for n > 1 are obtained using the extended transport approximation. That is, the number of neutrons scattered into group g is assumed to be equal to the number of neutrons scattered out from the group as

$$\sum_{g'} \Sigma^{n}_{s,g'\to g}\phi_{n,g'} = \Sigma^{n}_{s,g}\phi_{n,g}, \quad n>1. \tag{4.7}$$

Using Eq. (4.7) in Eq. (4.6), the consistent P_1 equation with the extended approximation can be obtained as

$$\begin{cases} iB\phi_{1,g} + \Sigma_{t,g}\phi_{0,g} = \sum_{g'} \Sigma_{s0,g'\to g}\phi_{0,g'} + \frac{1}{2}S_{f,g}, & n=0 \\ \frac{2}{3} iB\phi_{1,g} + \frac{1}{3} iB\phi_{0,g} + \Sigma_{t,g}\phi_{1,g} = \sum_{g'} \Sigma_{s0,g'\to g}\phi_{1,g'}, & n=1 \\ \frac{n+1}{2n+1} iB\phi_{n+1,g} + \frac{n}{2n+1} iB\phi_{n-1,g} & \\ \qquad + (\Sigma_{t,g} - \Sigma_{sn,g})\phi_{n,g} = 0, & n=2,3,\cdots,N-1 \\ \frac{N}{2N+1} iB\phi_{N-1,g} + (\Sigma_{t,g} - \Sigma_{sN,g})\phi_{N,g} = 0, & n=N \end{cases} \tag{4.8}$$

The last two equations in Eq. (4.8) can be solved successively from $n=N$, thus the consistent P_1 slowing down equations with the extended transport approximation of order N are solved as:

$$iB\phi_{1,g} + \Sigma_{t,g}\phi_{0,g} = \sum_{g'} \Sigma_{s0,g'\to g}\phi_{0,g'} + S_{f,g} \tag{4.9}$$

$$\frac{iB}{3}\phi_{0,g} + A_{1,g}\phi_{1,g} = \sum_{g'} \Sigma_{s1,g'\to g}\phi_{1,g'} \tag{4.10}$$

$$\phi_{n,g} = -\frac{n}{2n+1}\frac{iB}{A_{n,g}}\phi_{n-1,g}, \quad n = 2,3,\cdots N \tag{4.11}$$

where

$$A_{n,g} = b_{n-1,g} + \frac{a_n}{A_{n+1,g}} = b_{n-1,g} + \cfrac{a_n}{b_{n,g} + \cfrac{a_{n+1}}{b_{n+1,g} + \cfrac{a_{n+2}}{\cdots + \cfrac{a_{N-1}}{b_{N-1,g}}}}} \tag{4.12}$$

$$A_{N,g} = b_{n-1,g} \;\&\; b_{0,g} = \Sigma_{t,g} \tag{4.13}$$

$$a_n = \frac{n+1}{2n+1}\frac{n+1}{2(n+1)+1}B^2 \;\text{ and }\; b_{n,g} = \Sigma_{t,g} - \Sigma_{s,g}^{n+1}. \tag{4.14}$$

4.1.3. Critical Buckling Search and Fictitious Fission Source

The k-eigenvalue problem with Eq. (4.8) is solved with a default buckling value of 10^{-10} or a user-specified buckling value. Critical buckling search is also possible for super or sub productive compositions to obtain the fundamental mode spectrum. In this case, the critical buckling value is iteratively updated by using the linear interpolation of two latest buckling values until the multiplication factor converges to one. It is known that the fundamental mode spectrum with the critical buckling search gives a better weighting spectrum for generation of multigroup cross sections.

In case of non-fissionable material such as non-fuel assemblies in fast reactor, the eigenvalue problem should be solved with the external source. In this case, the fission spectrum of U-238 as default or a user-defined nuclide can be utilized as fictitious fission source. Additionally, the user can provide the external source instead of the fictitious fission source.

4.2. Collision Probability Method for 1D Cylindrical Geometry

4.2.1. Collision Probability Method for Cylindrical Geometry

The collision probability (CP) method used in EXUS-F is based on formulations for cylindrical geometry in Stamm'ler's book.

It is assumed that a cylindrical cell consists of n regions is given as shown in Figure 4-1 and the source density in each region is uniform and isotropic. Then, the neutron flux in region i, ϕ_i can be determined by introducing two types of response flux $X_i^k(\alpha)$ and $Y_i(\alpha)$ as:

$$\phi_i = Y_i(\alpha) j_{ext} + \sum_{k=1}^{n} X_i^k(\alpha) Q_k \tag{4.15}$$

where α is the albedo boundary condition, $Y_i(\alpha)$ is the current response flux caused by one neutron entering the cell uniformly with a cosine distribution, j_{ext} is the integrated partial in-current with a cosine distribution along the cell boundary S_B, $X_i^k(\alpha)$ is the source response flux in region i caused by a unit source density in region k, and Q is the source density. Note that both flux terms, $X_i^k(\alpha)$ and $Y_i(\alpha)$ take into account multiple reflections at the boundary which has an albedo α.

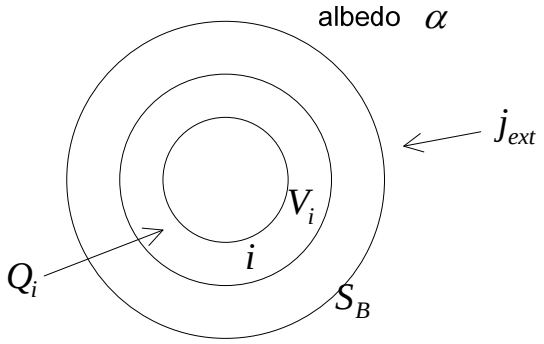

Figure 4-1. Cylindrical Geometry

The two response neutron fluxes can be expressed in terms of X_i^k , Y_i and α , where $X_i^k = X_i^k(0)$ and $Y_i = Y_i(0)$ are the basic response fluxes in black boundary condition ($\alpha = 0$).

First, the current response flux $Y_i(\alpha)$ can be represented with a multiplication factor by multiple reflections at the boundary surface. Γ is the absorption blackness of the cell and can be expressed in terms of Y_i.

$$\Gamma = \sum_{i=1}^{n} \Gamma_i = \sum_{i=1}^{n} \Sigma_{r,i} V_i Y_i \tag{4.16}$$

where Γ_i is the partial absorption blackness in region i, Σ_r is the removal cross section, and V is the volume of the region. If one neutron enters the cell, a fraction $(1-\Gamma)$ will reach the boundary surface and the fraction $\alpha(1-\Gamma)$ will be reflected and re-entered into the cell. Thus, each neutron that enters the cell for the first time contributes to the partial in-current with the amount of $1+\alpha(1-\Gamma)+\alpha^2(1-\Gamma)^2+\cdots$. The multiplication factor of the boundary is then $1/(1-(1-\Gamma)\alpha)$ and the current response flux $Y_i(\alpha)$ can be expressed as:

$$Y_i(\alpha) = \frac{Y_i}{1-(1-\Gamma)\alpha}. \tag{4.17}$$

By using Eq. (4.17), the source response flux $X_i^k(\alpha)$ can also be represented in terms of X_i^k . For the $X_i^k(\alpha)$, there is a contribution X_i^k from the source neutrons that never reached the boundary surface. There is V_k neutrons in region k and x_k neutrons reach the boundary surface from region k.

$$x_k = V_k P_k = \frac{S_B}{4\Sigma_{rk}} \Gamma_k = \frac{S_B}{4} V_k Y_k \tag{4.18}$$

where $P_k = S_B \Gamma_k / (4\Sigma_{rk} V_k)$ is the escape probability in region k. Then, αx_k neutrons are reflected and they can be treated as the incoming neutrons. It means they can contribute to $X_i^k(\alpha)$ as the current response flux. The source response flux $X_i^k(\alpha)$ is given by

$$X_i^k(\alpha) = X_i^k + \alpha x_k Y_i(\alpha) = X_i^k + \alpha x_k \frac{Y_i}{1-(1-\Gamma)\alpha} \tag{4.19}$$

Finally, the neutron flux can be expressed in terms of two basic response fluxes Y_i and X_i^k.

$$\phi_i = \frac{j_{ext} Y_i}{1-(1-\Gamma)\alpha} + \sum_{k=1}^{n} Q_k \left\{ X_i^k + \alpha x_k \frac{Y_i}{1-(1-\Gamma)\alpha} \right\} \tag{4.20}$$

There remains the problem of solving Y_i and X_i^k to determine the neutron flux and the set of balance equations can be introduced to obtain the two basic response fluxes.

$$\Sigma_{ti} \phi_i V_i = \sum_{j=1}^{n} P_{ji} (c_j \phi_j + \frac{Q_j}{\Sigma_{tj}}), \qquad i = 1, \cdots, n \tag{4.21}$$

where $P_{ji} = \tilde{P}_{ji} V_j \Sigma_j$, $\tilde{P}_{ji}$ is the collision probability which means the number of collisions in V_i caused by one neutron born inside V_j and $c_j = \Sigma_{sj} / \Sigma_{tj}$ is the self-scattering ratio.

X_i^k can be found by assuming no external current, $j_{ext} = 0$ and an unit source with the delta function, $Q_j = \delta_{ij}$. Then, Eq. (4.21) can be rewritten as:

$$\Sigma_{ti} V_i X_i^k = \sum_{j=1}^{n} P_{ji} c_j X_j^k + \frac{P_{ki}}{\Sigma_k} \tag{4.22}$$

Above equation can be re-written in the matrix form.

$$\begin{bmatrix} \Sigma_1 V_1 - P_{11}c_1 & -P_{21}c_2 & \cdots & -P_{n1}c_n \\ -P_{12}c_1 & \Sigma_2 V_2 - P_{22}c_2 & \cdots & -P_{n2}c_n \\ \vdots & \vdots & \ddots & \vdots \\ -P_{1n}c_1 & -P_{2n}c_n & \cdots & \Sigma_n V_n - P_{nn}c_n \end{bmatrix} \begin{bmatrix} X_1^k \\ X_2^k \\ \vdots \\ X_n^k \end{bmatrix} = \begin{bmatrix} \frac{P_{k1}}{\Sigma_k} \\ \frac{P_{k2}}{\Sigma_k} \\ \vdots \\ \frac{P_{kn}}{\Sigma_k} \end{bmatrix} \tag{4.23}$$

Similarly, Y_i can be obtained by assuming unit external current, $j_{ext}=1$ and no source. Then Eq. (4.21) can be expressed as:

$$\Sigma_{ti} V_i Y_i = \sum_{j=1}^{n} P_{ji} c_j Y_j + \gamma_i \tag{4.24}$$

where γ_i is the first flight collision blackness.

$$\gamma_i = \frac{4}{S_B}\left(\Sigma_{ti} V_i - \sum_{j=1}^{n} P_{ji} \right) \tag{4.25}$$

Eq. (4.24) can also be expressed in the matrix form as below.

$$\begin{bmatrix} \Sigma_1 V_1 - P_{11}c_1 & -P_{21}c_2 & \cdots & -P_{n1}c_n \\ -P_{12}c_1 & \Sigma_2 V_2 - P_{22}c_2 & \cdots & -P_{n2}c_n \\ \vdots & \vdots & \ddots & \vdots \\ -P_{1n}c_1 & -P_{2n}c_n & \cdots & \Sigma_n V_n - P_{nn}c_n \end{bmatrix} \begin{bmatrix} Y_1 \\ Y_2 \\ \vdots \\ Y_n \end{bmatrix} = \begin{bmatrix} \gamma_1 \\ \gamma_2 \\ \vdots \\ \gamma_n \end{bmatrix} \tag{4.26}$$

By solving Eqs. (4.23) and (4.26), the basic response fluxes with zero albedo Y_i and X_i^k are obtained. For these calculation, P_{ij} can be obtained using the Bickley function.

$$P_{ij} = \delta_{ij}\Sigma_i V_i + 2\left(S_{ij} + S_{i-1\,j-1} - (S_{i\,j-1} + S_{i-1\,j}) \right) \tag{4.27}$$

$$S_{ij} = \int_0^{R_i} \left(Ki_3(\tau_{ij}^+) - Ki_3(\tau_{ij}^-) \right) dy \tag{4.28}$$

$$Ki_n(x) = \int_0^{\frac{\pi}{2}} \cos^{n-1}\theta e^{-\frac{x}{\cos\theta}} d\theta \tag{4.29}$$

4.2.2. Regeneration of Higher Order Neutron Fluxes

Higher moments of the multigroup scattering matrix should be provided to handle the scattering anisotropic treatment. It means the higher moments of weighting spectrum in the ultrafine group level is necessary. However, the 0^{th} moment neutron flux is only solution from the collision probability method. To resolve this problem, the higher moment solutions from the homogenous mixture calculations are utilized to obtain the higher moment fluxes for the cylindrical geometry problem. The higher moment fluxes in the cylindrical geometry is determined as follows:

$$\phi_{l,cyl} = \frac{\phi_{0,cyl}}{\phi_{0,\mathrm{hom}}} \phi_{l,\mathrm{hom}} \tag{4.30}$$

where, $\phi_{0,cyl}$ is the 0^{th} order neutron flux from the collision probability method, and $\phi_{0,\mathrm{hom}}$ and $\phi_{l,\mathrm{hom}}$ are 0^{th} order and 1^{st} order neutron fluxes by solving the consistent P_n equations with the N-th order extended approximation.

4.3. Method of Characteristic for 2D Hexagonal Geometry

The two-dimensional (2D) MOC solver of nTRACER for hexagonal geometry problems is incorporated into EXUS-F for lattice calculations for assemblies and 2D core problems. The MOC solver has an advantage to incorporate the high order moments of the scattering source with ease for the transport problem.

4.3.1. MOC Solution for 2D Problems

The Boltzmann transport equation for two-dimensional problems is given by

$$\cos\alpha\sin\theta\frac{\partial}{\partial x}\varphi(x,y,\hat{\Omega})+\sin\alpha\sin\theta\frac{\partial}{\partial y}\varphi(x,y,\hat{\Omega}) \\ +\Sigma_t(x,y)\varphi(x,y,\hat{\Omega})=Q(x,y,\hat{\Omega}) \tag{4.31}$$

where α is the azimuthal angle and θ is the polar angle. Eq. (4.31) can be rewritten in the general form of 1st order partial differential equation.

$$(\cos\alpha\sin\theta,\sin\alpha\sin\theta,Q-\Sigma_t\varphi)\cdot(\frac{\partial}{\partial x}\varphi,\frac{\partial}{\partial y}\varphi,-1)=0 \tag{4.32}$$

By using the Method of Characteristic of PDE, the solution of the transport equation can be obtained from a set of 3 equations for characteristic curve. The equations of curve are expressed as below:

$$\begin{cases}\dfrac{dx}{ds}=\cos\alpha\sin\theta \\ \dfrac{dy}{ds}=\sin\alpha\sin\theta \\ \dfrac{d\varphi}{ds}=Q(s)-\Sigma_t(s)\varphi(s)\end{cases} \tag{4.33}$$

where s is an arc length of the projected characteristic curve. It can be assumed that the source term Q and the total cross section are constant in very small region. The solution of the above equations can be obtained as follows:

$$\begin{cases}\dfrac{dx}{ds}=\cos\alpha\sin\theta & \rightarrow\ x-x_0=\cos\alpha\sin\theta s \\ \dfrac{dy}{ds}=\sin\alpha\sin\theta & \rightarrow\ y-y_0=\sin\alpha\sin\theta s \\ \dfrac{d\varphi}{ds}=Q-\Sigma_t\varphi & \rightarrow\ \varphi(s)=\varphi(0)e^{-\Sigma_t s}+\dfrac{Q}{\Sigma_t}(1-e^{-\Sigma_t s})\end{cases} \tag{4.34}$$

The curve equation can be rewritten in terms of distance from the origin (x_0, y_0).

$$\begin{aligned}(x-x_0)^2+(y-y_0)^2 &= (\cos^2\alpha+\sin^2\alpha)\sin^2\theta s^2 \\ &= l^2\end{aligned} \tag{4.35}$$

$$\therefore s = \frac{l}{\sin\theta} \tag{4.36}$$

Finally, the angular flux in 2D problems can be determined using Eqs. (4.34) and (4.36) as below.

$$\varphi(l) = \varphi(0)e^{-\frac{\Sigma_t l}{\sin\theta}} + \frac{Q}{\Sigma_t}(1-e^{-\frac{\Sigma_t l}{\sin\theta}}) \tag{4.37}$$

4.3.2. Anisotropic Scattering Treatment

For the MOC solver, the function to calculate the high order moments of the scattering source up to third order is implemented based on Ryu's method[21]. The higher order moments of the scattering source can be derived from the expansion of the angular flux in terms of the spherical harmonics. With the spherical harmonics function, the high order angular flux moment is given by

$$\phi_l^m(\vec{r},E) = \int_{-1}^{+1}\int_0^{2\pi}\varphi(\vec{r},E,\hat{\Omega})Y_{lm}^*(\mu',\alpha')d\alpha' d\mu' \tag{4.38}$$

where $\mu = \cos\theta$. For example, 1st order of the scattering source can be expressed as:

$$\begin{aligned}&S_1(\vec{r},E,\hat{\Omega}) = S_{1,0}(\vec{r},E,\hat{\Omega}) + S_{1,-1}(\vec{r},E,\hat{\Omega}) + S_{1,1}(\vec{r},E,\hat{\Omega}) \\ &= \frac{3}{4\pi}\int_{E'}\Sigma_{s,l}(\vec{r},E'\to E)\int_{-1}^{+1}\int_0^{2\pi}\begin{pmatrix}\cos\theta'\cos\theta \\ +\sin\theta'\sin\theta\cos\alpha'\cos\theta \\ +\sin\theta'\sin\theta\sin\alpha'\sin\alpha\end{pmatrix}\varphi(\vec{r},E',\hat{\Omega}')d\alpha' d\mu' dE'\end{aligned} \tag{4.39}$$

4.3.3. Regeneration of Higher Order Neutron Fluxes

From the MOC calculation with the scattering order *n*, *(2n+1)*

angular flux moments are given. Thus, the n-th moment of the scattering cross section from broad group G' to G can be defined using the spherical harmonics as below:

$$\Sigma^n_{G'\to G}(\hat{\Omega}) = \frac{\sum_{g\in G}\sum_{g'\in G'} \Sigma^n_{g'\to g} \sum_{m=-n}^{n} \phi^m_{n,g'} Y_{n,m}(\hat{\Omega})}{\sum_{g'\in G'}\sum_{m=-n}^{n} \phi^m_{n,g'} Y_{n,m}(\hat{\Omega})}. \tag{4.40}$$

However, the broad group scattering cross section in Eq. (4.40) has a dependency on the incident neutron angle. To remove this dependency, higher order weighting function $\phi_{n,g}$ is defined as below.

$$\phi_{n,g} = \sqrt{\sum_{m=-n}^{n} \left(\phi^m_{n,g}\right)^2} \tag{4.41}$$

With the re-defined weighting function, the broad group scattering cross section can be determined as:

$$\Sigma^n_{G'\to G} = \frac{\sum_{g\in G}\sum_{g'\in G'} \Sigma^n_{g'\to g}\phi_{n,g'}}{\sum_{g'\in G'} \phi_{n,g'}}. \tag{4.42}$$

4.4. Group Condensation

From the UFG transport calculation, the 0^{th} moment neutron flux and higher moment weighting spectrum are obtained to generate the broad group cross section. Note that the broad group structure can be determined by the user, but the broad group boundaries should be chosen as a subset of the UFG boundaries.

The broad group cross section for most reactions are obtained by averaging the UFG cross section with the 0^{th} moment neutron

flux as the weighting spectrum.

$$\sigma_{x,G} = \frac{\sum_{g \in G} \sigma_{x,g} \phi_g}{\sum_{g \in G} \phi_g} \tag{4.43}$$

where, x is an index for reaction like total, capture and scattering.

The broad group scattering transfer matrix can also be determined using the UFG solution. For higher order moments of the scattering matrix, the higher moment neutron fluxes are used as the weighting function. An element of the n−th order scattering transfer matrix is obtained as below.

$$\sigma^n_{G' \to G} = \frac{\sum_{g \in G} \sum_{g' \in G'} \sigma^n_{g' \to g} \phi_{n,g'}}{\sum_{g' \in G'} \phi_{n,g'}} \tag{4.44}$$

The broad group fission spectrum vector χ_G which have no dependency on incident group G' can be calculated from the UFG fission spectrum matrix $\chi_{g' \to g}$ using the 0^{th} moment neutron flux.

$$\chi_G = \frac{\sum_{g'=1}^{NUFG} \sigma_{f,g'} \phi_{g'} \sum_{g \in G} \chi_{g' \to g}}{\sum_{g'=1}^{NUFG} \sigma_{f,g'} \phi_{g'}} \tag{4.45}$$

Chapter 5. Numerical Results

5.1. Verification Tests of EXUS-F

The functionality of EXUS-F was first tested using two sets of problems. One is the set of 0D homogeneous mixture problems and the other is the set of cylindrical pin-cell problems. The problems were derived from the fuel assemblies of the ABR 1000 benchmark problems[22] as shown in Table 5-1. The 0D mixture problems were prepared by homogenizing all the composition in each assembly, whereas the 1D cylindrical pin-cell problems were derived by converting a single hexagonal pin cell problem. All EXUS-F calculations were performed based on the ENDF/B-VII.0 and JENDL 4.0 libraries. For verification tests, a broad group structure consist of 47 groups was defined. Each broad group consists of 40 ultrafine groups except few groups under 200 eV, which consists of 60 ultrafine groups. Results of EXUS-F were compared with the references solutions obtained from continuous energy Monte Carlo calculations with the McCARD code[23] developed at SNU. The McCARD calculations were performed with 100,000 particles per each cycle, 100 inactive cycles and 1,000 active cycles based on the ENDF/B VII.0 and JENDL 4.0 libraries.

Table 5-1. Problem Sets for EXUS-F Verification Tests

Case	Assembly Type
Case 1	ABR1000 Metallic Inner Core
Case 2	ABR1000 Metallic Inner Core
Case 3	ABR1000 Oxide Inner Core
Case 4	ABR1000 Oxide Middle Core
Case 5	ABR1000 Oxide Outer Core

5.1.1. Homogenous Mixture Problems with ENDF/B-VII.0

Table 5-2 compares the infinite multiplication factors of McCARD and EXUS-F for the homogeneous mixture problems with the ENDF/B-VII.0 library. EXUS-F slightly overestimates the infinite multiplication factor relative to McCARD, but EXUS-F values agree very well with McCARD solutions within ~50 pcm. The broad-group neutron flux spectrum of EXUS-F also agree very well with the McCARD result, as shown in Figure 5-1 for Case 1. The broad-group cross sections were also compared for Fe-56 and Cr-52, because they have resonance-like XSs in the fast energy range. Figure 5-2 and Figure 5-3 compare the 47G total XSs of Case 1 for Fe-56 and Cr-52, respectively. The broad-group XSs of EXUS-F agree very well with the reference results. The maximum difference in the total XS is 0.1% for Fe-56 and 0.2% for Cr-52.

Table 5-2. Infinite Multiplication Factors of McCARD and EXUS-F for Homogenous Mixture Problems with ENDF/B-VII.0 Library

	Case 1	Case 2	Case 3	Case 4	Case 5
McCARD	1.28914	1.47828	1.15217	1.22727	1.38350
EXUS-F	1.28982	1.47904	1.15289	1.22797	1.38431
Reactivity Diff. [pcm]	41	35	54	46	42

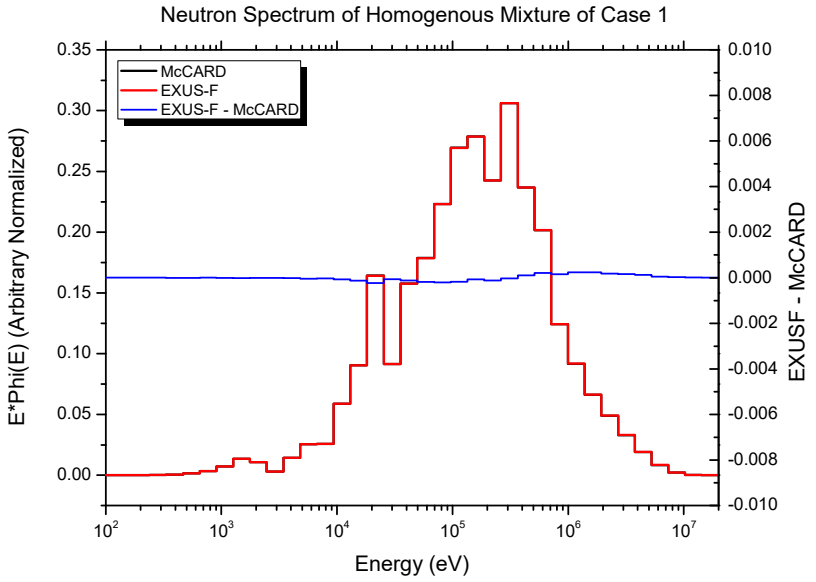

Figure 5-1. Broad-Group Neutron Spectrum of Homogenous Mixture Problem of Case 1 with ENDF/B-VII.0 Library

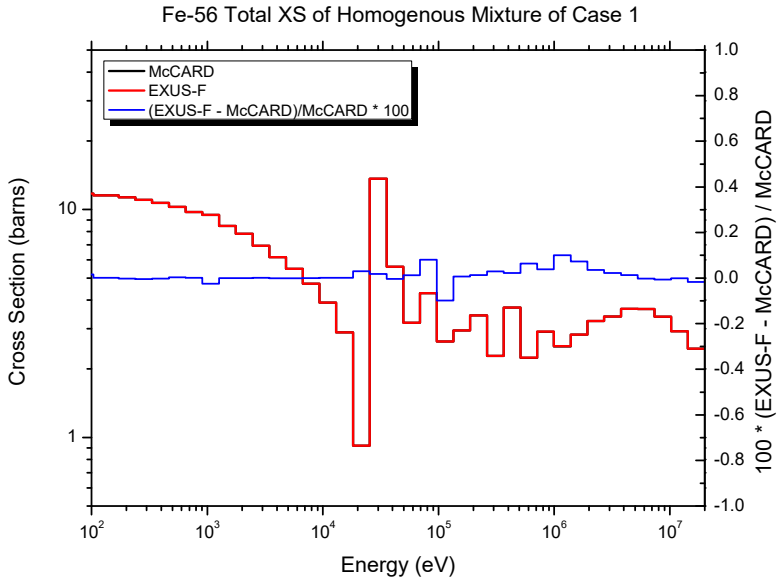

Figure 5-2. Broad-Group Fe-56 Total Cross Section of Homogenous Mixture Problem of Case 1 with ENDF/B-VII.0 Library

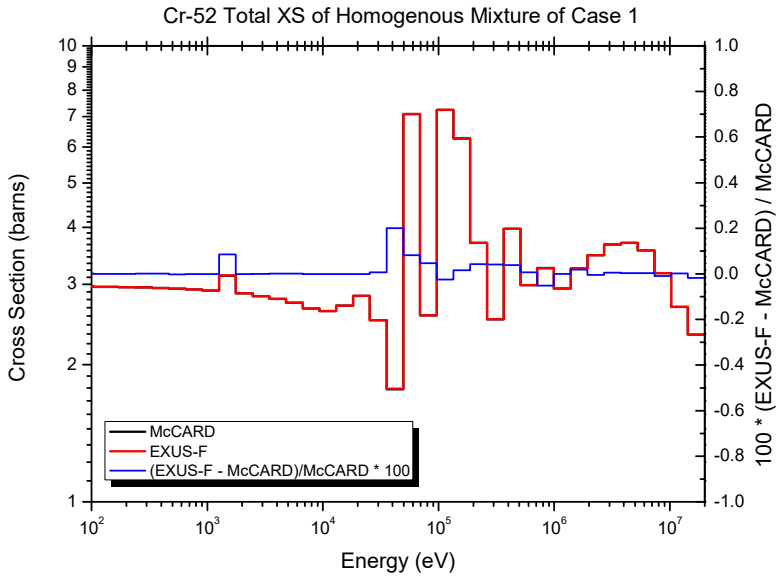

Figure 5-3. Broad-Group Cr-52 Total Cross Section of Homogeneous Mixture Problem of Case 1 with ENDF/B-VII.0 Library

5.1.2. Homogenous Mixture Problems with JENDL 4.0

To verify the capability of processing general ENDF format nuclear data libraries, the same 0D mixture problems was repeated with the JENDL 4.0 library. Table 5-3 shows the infinite multiplication factors from McCARD and EXUS-F calculations. The McCARD multiplication factors obtained with the JENDL 4.0 library is 650 pcm – 700 pcm larger for Cases 1 and 2 and 150 pcm – 250 pcm smaller for Cases 3 through 5 than those with ENDF/B-VII.0 in Table 5-2. Similarly, the nTRACER multiplication factors are overestimated in Case 1 and 2 and underestimated din Case 3 – 5, compared with those with the ENDF/B-VII.0 library. The reactivity differences between McCARD and EXUS-F are observed within ~ 60 pcm. As shown in Figure 5-4 through Figure 5-6, the broad group neutron spectrum and XSs are matched very well with the reference. From Figure 5-3 and Figure 5-6, it can be noted that the multigroup XS of Cr-52 have different value for left wing of the main resonance of Cr-52 scattering XS. It means the pointwise XSs in both nuclear data libraries are different and the difference makes the above mentioned difference in the multiplication factor.

Table 5-3. Infinite Multiplication Factors of McCARD and EXUS-F for Homogenous Mixture Problems with JENDL 4.0 Library

	Case 1	Case 2	Case 3	Case 4	Case 5
McCARD	1.29632	1.48486	1.15044	1.22506	1.38068
EXUS-F	1.29692	1.48556	1.15134	1.22593	1.38170
Reactivity Diff. [pcm]	36	32	68	58	53

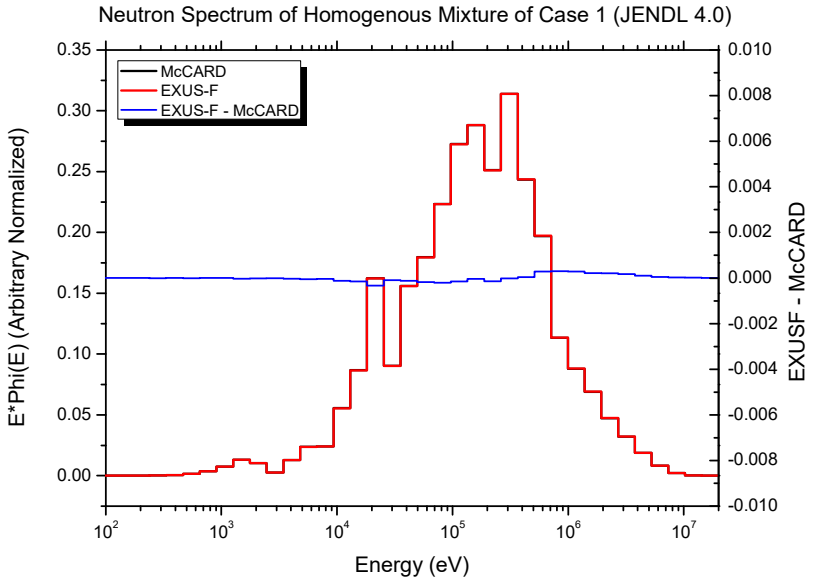

Figure 5-4. Broad-Group Neutron Spectrum of Homogenous Mixture Problem of Case 1 with JENDL 4.0 Library

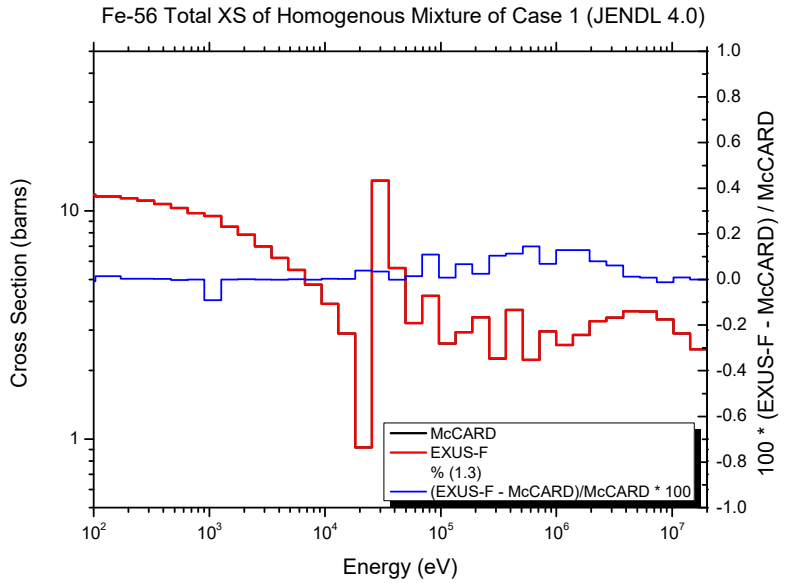

Figure 5-5. Broad-Group Fe-56 Total Cross Section of Homogenous Mixture Problem of Case 1 with JENDL 4.0 Library

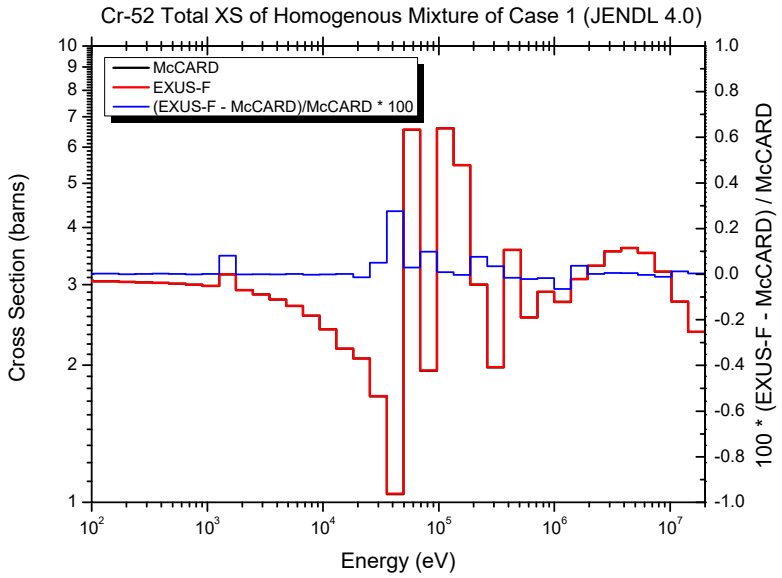

Figure 5-6. Broad-Group Cr-52 Total Cross Section of Homogenous Mixture Problem of Case 1 with JENDL 4.0 Library

5.1.3. Cylindrical Fuel Pin Cell Problems with ENDF/B-VII.0

Table 5-4 compares the infinite multiplication factors from the EXUS-F and McCARD calculations for the cylindrical pin-cell problems using the ENDF/B-VII.0 library. It can be seen that the multiplication factors of EXUS-F match well the McCARD reference solutions, although EXUS-F shows a slightly positive reactivity bias as for the homogeneous mixture problems. Figure 5-7 and Figure 5-8 show the broad-group neutron spectra obtained from EXUS-F and McCARD calculations in the fuel and cladding regions, respectively. The neutron spectra from EXUS-F and McCARD are almost identical in both regions. The broad-group total XS of Fe-56 and Cr-52 in the cladding region are shown in Figure 5-9 and Figure 5-10. It can be seen that the broad-group cross sections of Fe-56 and Cr-52 obtained from EXUS-F agree well with the reference McCARD results, except for ~1.3% error in the total XS of Cr-52 in the group including the Cr-52 resonance at 1.63 keV. Although this error does not affect the reactivity noticeably, further investigation is needed to identify the reason for this relatively large error.

Table 5-4. Infinite Multiplication factors from McCARD and nTRACER in Cylindrical problems with ENDF/B-VII.0 Library

	Case 1	Case 2	Case 3	Case 4	Case 5
McCARD	1.38299	1.57474	1.21551	1.29253	1.45313
EXUS-F	1.38364	1.57546	1.21648	1.29351	1.45414
Reactivity Diff. [pcm]	34	29	66	59	48

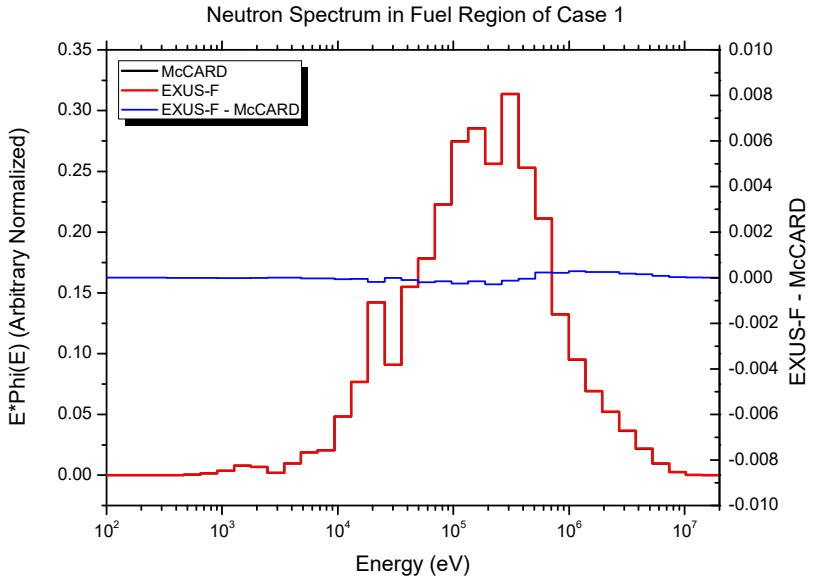

Figure 5-7. Broad-Group Neutron Spectrum in Fuel Region of Pin-Cell Problem of Case 1 with ENDF/B-VII.0 Library

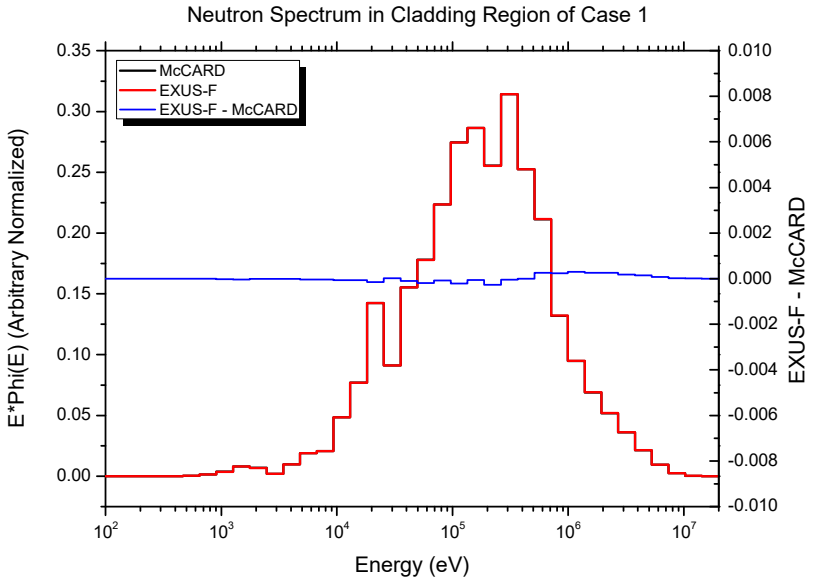

Figure 5-8. Broad-Group Neutron Spectrum in Cladding Region of Pin-Cell Problem of Case 1 with ENDF/B-VII.0 Library

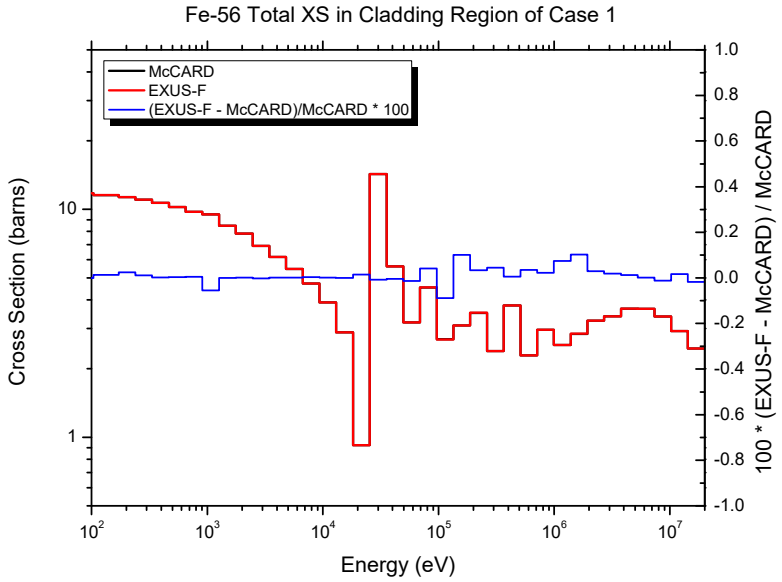

Figure 5-9. Broad-Group Fe-56 Total Cross Section in Cladding Region of Pin-Cell Problem of Case 1 with ENDF/B-VII.0 Library

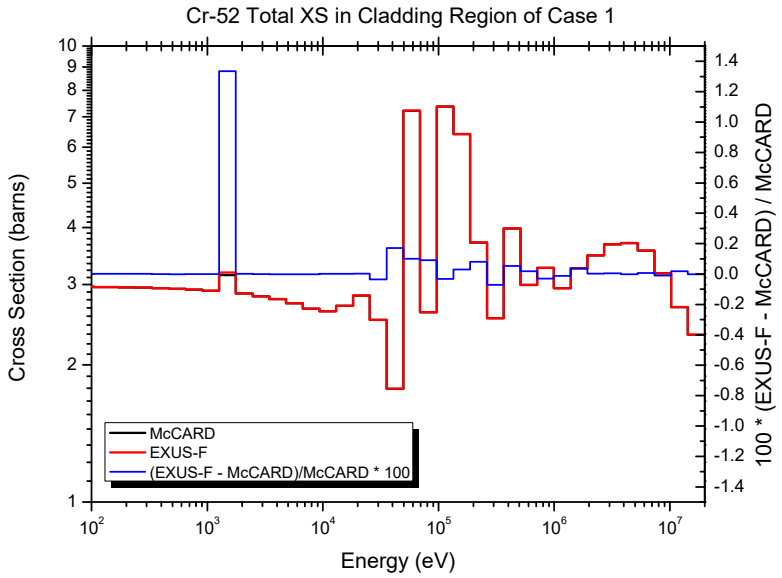

Figure 5-10. Broad-Group Cr-52 Total Cross Section in Cladding Region of Pin-Cell Problem of Case 1 with ENDF/B-VII.0 Library

5.1.4. Cylindrical Fuel Pin Cell Problems with JENDL 4.0

Table 5-5 shows the multiplication factors from the EXUS-F and McCARD calculations for the cylindrical pin-cell problems using the JENDL 4.0 library and their reactivity differences. The multiplication factors from EXUS-F are slightly larger than these from McCARD. Similar to the 0D mixture problems, the multiplication factors are overestimated in Cases 1 and 2 and they are underestimated in Case 3 through Case 5. The neutron spectra and the braod-group total XSs also show similar tendency. The neutron spectra from EXUS-F and McCARD are almost identical in both regions. In total XS of Cr-52 of Figure 5-14, ~1.3% error in Figure 5-10 is also observed in the same group including the Cr-52 resonance at 1.63 keV. From these results, it can be said that the versatility of EXUS-F which can use any nuclear data set as long as the set is given in the ENDF format is proved useful.

Table 5-5. Infinite Multiplication factors from McCARD and nTRACER in Cylindrical problems with JENDL 4.0 Library

	Case 1	Case 2	Case 3	Case 4	Case 5
McCARD	1.38299	1.57474	1.21551	1.29253	1.45313
EXUS-F	1.38364	1.57546	1.21648	1.29351	1.45414
Reactivity Diff. [pcm]	34	29	66	59	48

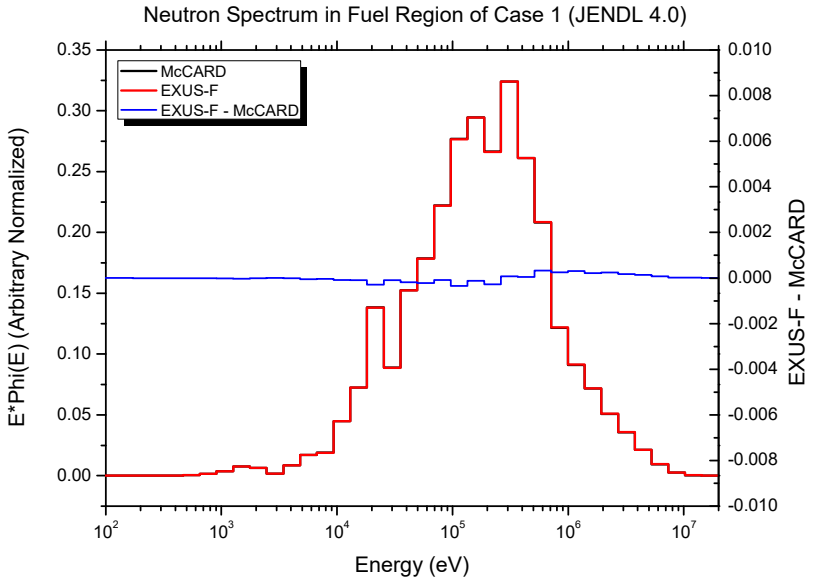

Figure 5-11. Broad-Group Neutron Spectrum in Fuel Region of Pin-Cell Problem of Case 1 with JENDL 4.0 Library

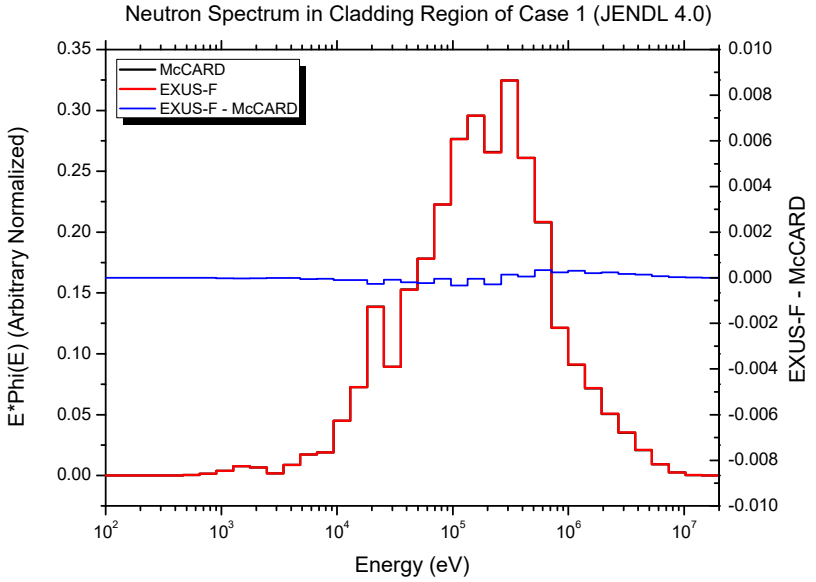

Figure 5-12. Broad-Group Neutron Spectrum in Cladding Region of Pin-Cell Problem of Case 1 with JENDL 4.0 Library

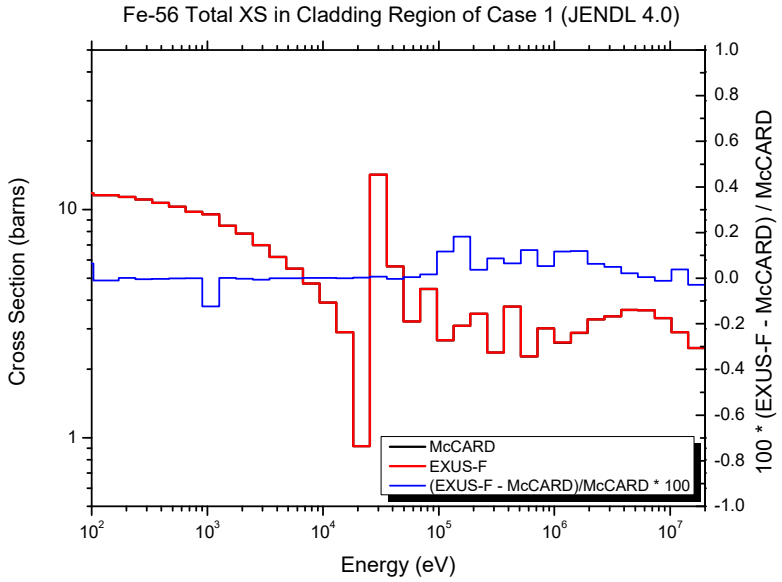

Figure 5-13. Broad-Group Fe-56 Total Cross Section in Cladding Region of Pin-Cell Problem of Case 1 with JENDL 4.0 Library

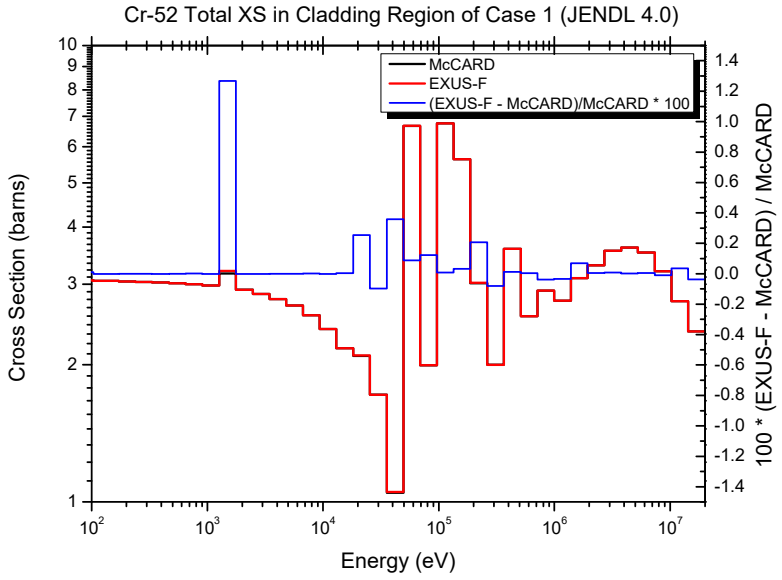

Figure 5-14. Broad-Group Cr-52 Total Cross Section in Cladding Region of Pin-Cell Problem of Case 1 with JENDL 4.0 Library

5.2.Verification Tests of EXUS-F/nTRACER Calculations

Verification tests were performed for the whole core calculation capability of the EXUS-F/nTRACER system using the metallic fuel core design of the 1000 MWth Advanced Burner Reactor (ABR 1000) [22]. Two-dimensional slice model was used in these tests instead of a full 3D model. Figure 5-15 shows the radial core layout of the ABR 1000 metallic fuel core. The core configuration of control assembly out was used with coolant and duct in the primary and secondary control assembly positions. The fuel compositions at the beginning of cycle (BOC) were used with an explicit geometry core model without any homogenization.

The MG XSs for 2D core calculations with nTRACER were generated using EXUS-F. Different sets of MG XSs were generated in the aforementioned 47G structure by changing the calculation condition in EXUS-F. The 47G cross sections for non-fuel assemblies were generated by performing slowing calculations for homogeneous mixtures. For fuel assemblies, a cylindrical assembly model was derived based on preliminary Monte Carlo calculations and the slowing down calculations were performed using the CP method. In addition, a 2D MOC core calculation with homogenized assembly models was performed in EXUS-F calculation to consider the region-to-region spectrum transition effects. Figure 5-16 shows the calculation procedure of EXUS-F/nTRACER calculation.

Reference solutions were obtained from continuous energy Monte Carlo calculations with the McCARD code. Continuous cross section data were prepared using the NJOY code using the same evaluated nuclear data files. McCARD calculations were performed to yield small uncertainties, specifically standard deviations smaller than 2 pcm for multiplication factor and 0.1% for cross section and fission power tallies.

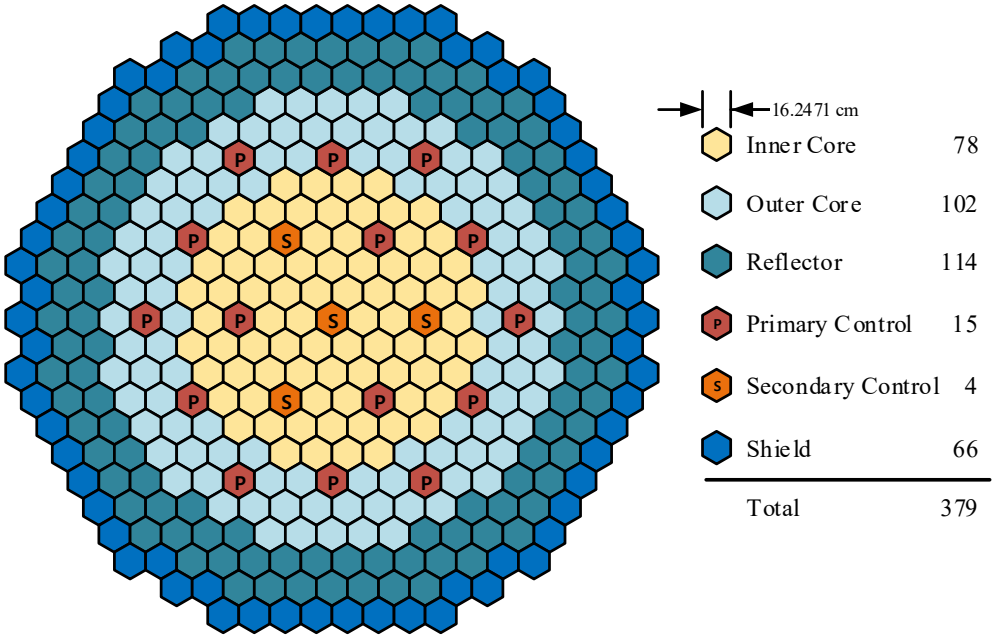

Figure 5-15. Radial Core Layout of ABR 1000 Metallic Fuel Core

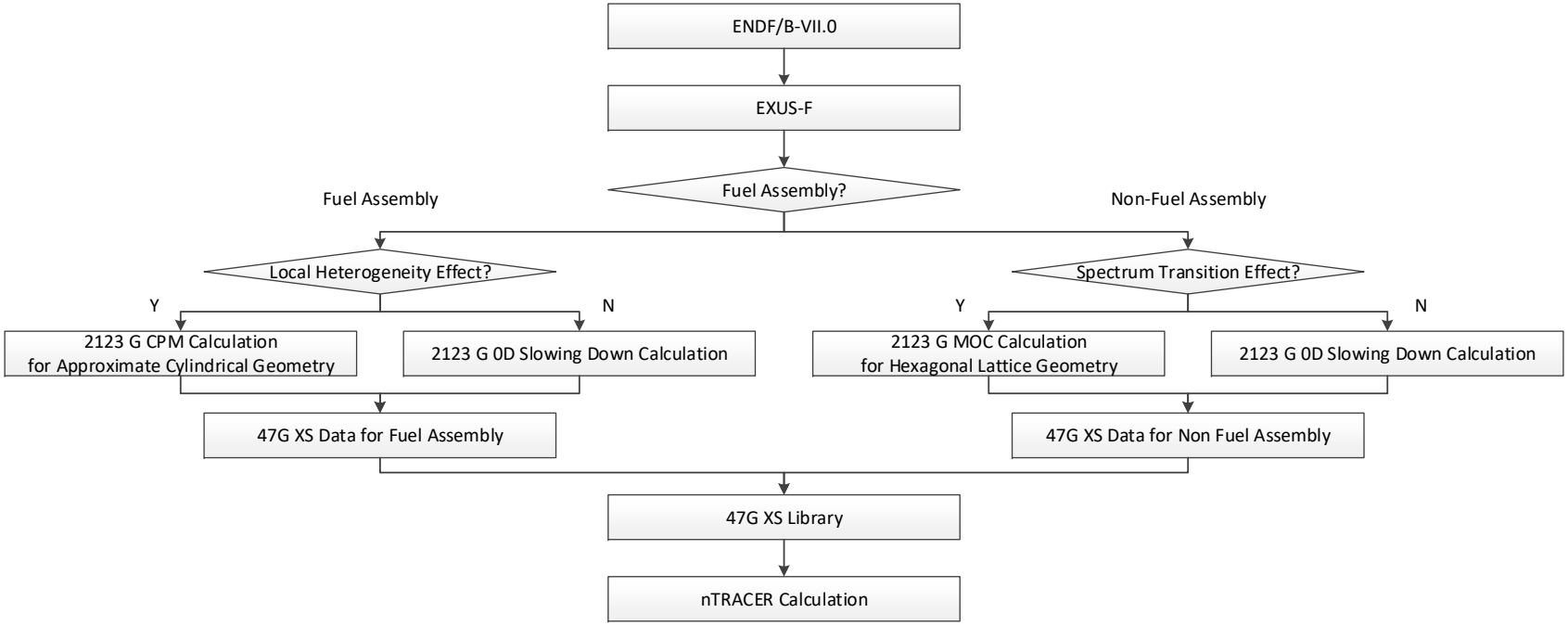

Figure 5-16. EXUS-F/nTRACER Calculation Procedure for Explicit Geometry Whole-Core Calculation

5.2.1. Determination of Approximate Model for Fuel Assembly XS Generation

The main goal of the EXUS-F/nTRACER system is to perform whole core transport calculation with explicit geometry modeling. This requires to generate MG XSs for individual materials such as fuel, cladding and coolant by considering the local heterogeneity effects. The best approach to achieve this goal would be to perform the UFG slowing down calculation using the as-built assembly model and calculate the MG XS based on the exact solution. However, the UFG slowing down calculation for the as-built model requires an excessive computational time. Therefore, cylindrical pin and assembly models were developed for fuel assemblies.

Figure 5-17 shows the assembly configuration of the ABR 1000 core model and two approximate cylindrical models. The pin-cell model was developed by adding two annuli for the assembly duct and inter-assembly gap to a single pin model. The radii of the two annuli were determined to conserve component volume fractions in the assembly. The other assembly model was developed to preserve component volumes instead of volume fractions, but the fuel, cladding and coolant inside the duct were homogenized.

To determine a proper approximate model, preliminary Monte Carlo calculations were performed with McCARD for the assembly with explicit geometry, a homogeneous mixture model and two approximate cylindrical models. The McCARD calculations were performed with 100,000 particles per each cycle, 100 inactive cycles and 1,000 active cycles based on the continuous energy ENDF/B VII.0 library.

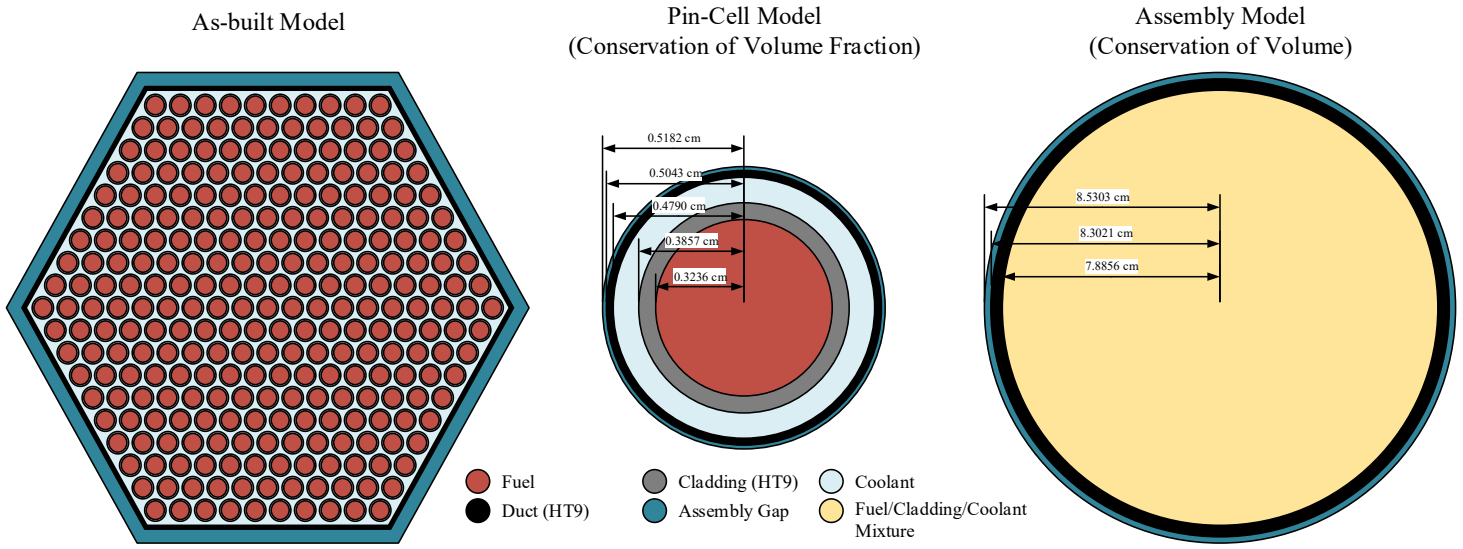

Figure 5-17. Assembly Geometry of ABR 1000 Metallic Core and Approximate Cylindrical Models for MG XS Generation with EXUS-F

Figure 5-18 through Figure 5-21 show 47G total XSs of representative isotopes in five different regions of a fuel assembly obtained with the as-built assembly model and the relative differences of the corresponding XSs obtained with approximate models. All the XSs were determined from the McCARD calculations and the relative differences of the cross sections calculated with approximate models were determined relative to the results obtained with the explicit assembly model as:

$$\text{Rel. Diff. of Total XS} = \frac{\sigma_{t,\text{approximate model}} - \sigma_{t,\text{explicit model}}}{\sigma_{t,\text{explicit model}}} \times 100 . \qquad (5.1)$$

As shown in the Figure 5-21, the total XSs calculated with the cylindrical assembly model agree very well with those obtained with the as-built assembly model for all five regions, except for ~6% discrepancy in U-238 XS of fuel region in the group containing the Na-23 resonance at 2.81 KeV. The U-238 cross section error is caused by the homogenization of the inside of the duct but its impact on reactivity is not significant because of low neutron population in this group due to the huge Na-23 resonance. The cylindrical pin and homogeneous mixture models show similar error trends for the Fe-56 XSs in cladding and duct regions. The homogeneous mixture model shows large discrepancies in the U-238 total XS in fuel region relative to the cylindrical pin and assembly models. All the three approximate models produce accurate Na-23 cross sections. Based on these results, the cylindrical assembly model was selected for the fuel assembly model for MG XS generation.

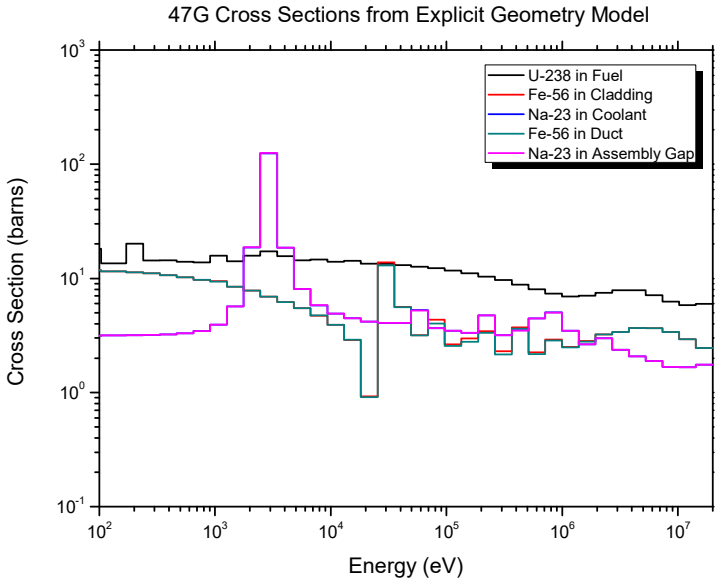

Figure 5-18. 47G Total XSs of U-238 in Fuel, Fe-56 in Cladding, Na-23 in Coolant, Fe-56 in Duct and Na-23 in Inter-assembly Gap Obtained with As-built Assembly Model

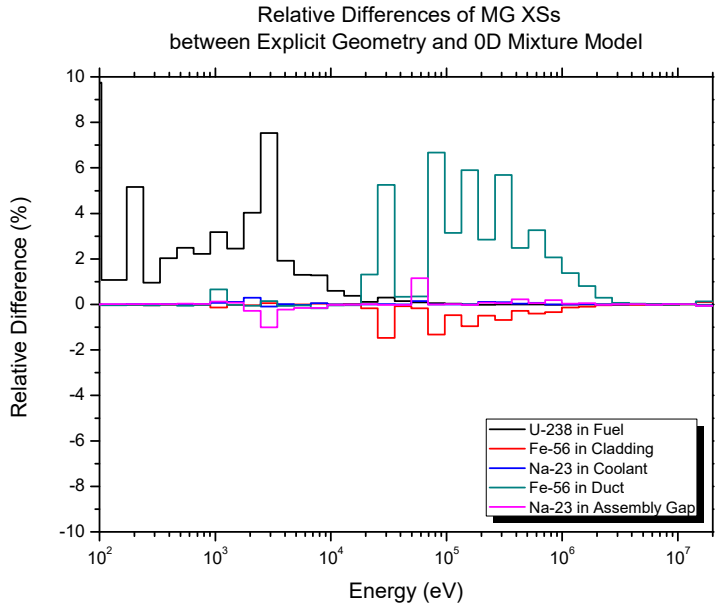

Figure 5-19. Relative Differences of Total Cross Sections of Representative Isotopes in Each Region Obtained with Homogeneous Mixture Model

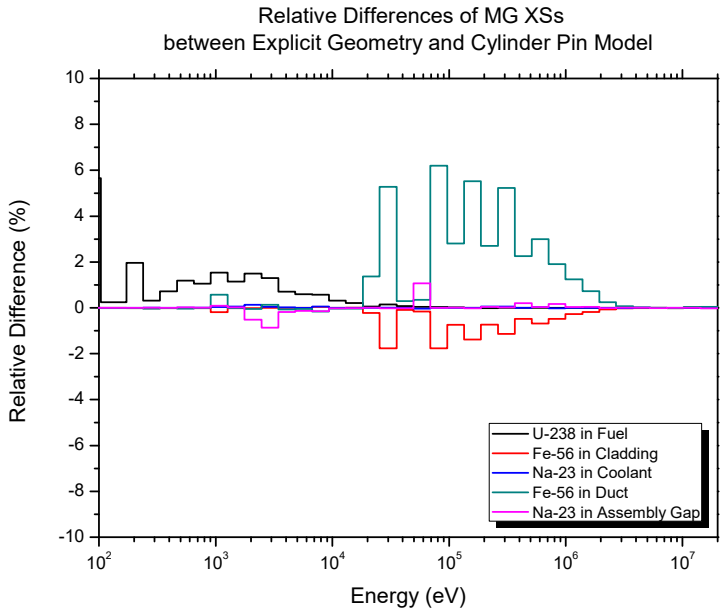

Figure 5-20. Relative Differences of Total Cross Sections of Representative Isotopes in Each Region Obtained with Cylindrical Pin Model

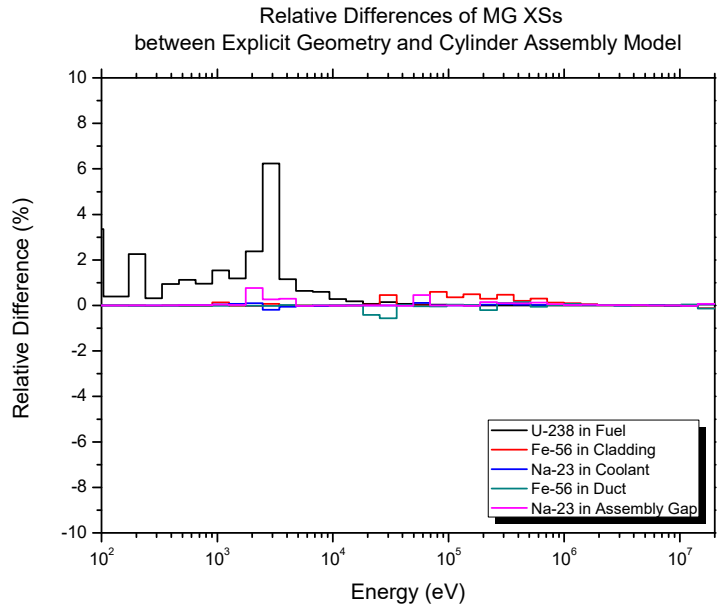

Figure 5-21. Relative Differences of Total Cross Sections of Representative Isotopes in Each Region Obtained with Cylindrical Assembly Model

5.2.2. Comparison of Assembly Calculation Results between nTRACER and McCARD

Three sets of 47G XS data were prepared for inner and outer core assemblies of the ABR 1000 metallic core from the EXUS-F UFG slowing down calculations with the ENDF/B-VII.0 library and the aforementioned three approximate models. Using these 47G cross section sets, nTRACER calculations were performed for two single assembly problems. The 2D MOC calculations with nTRACER were performed with the following parameters: 24 azimuthal angles in 180 degrees, 4 polar angles in 90 degrees, 0.05 cm ray spacing, and 3rd order anisotropic scattering treatment.

Table 5-6 compares the multiplication factors obtained from McCARD and nTRACER calculations for the inner and outer core assemblies. It can be seen that the multiplication factors of nTRACER agree well with the reference McCARD solutions with all three sets of XSs, although the XS sets obtained with pin and assembly models yield slightly better results than that obtained with the homogeneous mixture model. The overestimated total XS of Fe-56 in the duct region of the pin model results in a small negative bias in the multiplication factor compared to the assembly model. The use of the XS set obtained with the homogeneous mixture model yields underestimated multiplication factors because of overestimated XS of U-238 in the fuel region.

Table 5-6. Multiplication Factor Results of EXUS-F/nTRACER for Assembly Problems

Assembly Type	Inner Core Assembly		Outer Core Assembly	
McCARD (Ref.)	1.29386 ± 7 pcm		1.48257 ± 7 pcm	
nTRACER (Approximate Model)	k_{eff}	Reactivity Diff.* [pcm]	k_{eff}	Reactivity Diff. [pcm]
Mixture	1.29263	−74	1.48178	−36
Pin Model	1.29371	−9	1.48265	4
Assembly Model	1.29410	14	1.48306	22

*Reactivity Difference: $\rho_{nTRACER} - \rho_{McCARD} = (1/k_{eff,McCARD} - 1/k_{eff,nTRACER})$

5.2.3. 2D Core Calculation without Considering Spectrum Transition Effects

For the 2D core calculation with nTRACER for ABR 1000 metallic fuel core, 47G XS data was prepared from the EXUS-F calculation. For each of two types of fuel assemblies, XSs were generated using the cylindrical assembly model. The cross sections of non-fuel assemblies such as reflector, shield, and control assembly were generated by performing the slowing calculations for the homogeneous mixture of each single assembly. The fission matrix of U-238 which is the most abundant fissionable nuclide in the core was used as the fission source. However, it is noted that the neuron spectra in non-fuel assemblies are largely determined by the leaking-in neutron source from neighboring assemblies. In addition, the MG cross section generation with single assembly models only completely neglects the region-to-region spectral transition effects.

The nTRACER calculations were performed using the following parameters: 24 azimuthal angles in 180 degrees, 4 polar angles in 90 degrees, 0.05 cm ray spacing, and 3rd order anisotropic scattering treatment. The McCARD continuous energy Monte Carlo calculation was performed to obtain the reference solution. The McCARD calculation was performed with 200,000 particles per cycle, 2,000 active cycles and 500 inactive cycles. Pin power distributions were tallied from the McCARD calculation with 0.1% maximum relative error.

Table 5-7 compares the multiplication factors and pin power distributions of the 2D core problem of ABR 1000 obtained from the EXUS-F/nTRACER and McCARD calculations as a function of anisotropic scattering order. Detailed pin power distribution in a 1/6 core model and pin power differences between nTRACER and McCARD are shown in Figure 5-22 through Figure 5-26, respectively. It can be seen from Table 5-7 that the neglect of anisotropic scattering introduces large discrepancies in the multiplication factor and the pin power distribution. These discrepancies are reduced drastically by introducing the transport

correction method. Note that a definition of the transport cross section in the nTRACER calculation is written as:

$$\sigma_{tr,g} = \sigma_{t,g} - \sigma_{s1,g} \tag{5.2}$$

where $\sigma_{tr,g}$ and $\sigma_{s1,g}$ are the transport XS of group g and the 1st order anisotropic scattering XS, respectibly. The multiplication factors and pin power distributions become slightly closer to the reference solutions when higher order anisotropic scattering cross sections are used instead of the transport cross section. It is noted that the EXUS-F/nTRACER calculation always overestimates the multiplication factors about 250 pcm even with the anisotropic scattering. A global tilt in pin power distribution is also observed. The pin power is overestimated at the core periphery but underestimated at the core center.

Table 5-7. nTRACER Results of 2D Core Problem vs. Anisotropic Scattering Order

McCARD (Ref.)	1.21958 ± 2 pcm			
nTRACER (Scattering Order)	k_{eff}	Reactivity Diff.* [pcm]	Max. Pin Power Difference** [%]	RMS. Pin Power Difference [%]
0^{th} order	1.23860	1259	7.54	2.95
0^{th} order with Tr corr.	1.22392	291	2.72	1.21
1^{st} order	1.22314	239	2.61	1.02
2^{nd} order	1.22367	274	2.67	1.13
3^{rd} order	1.22355	266	2.65	1.12

* Reactivity Difference: $\rho_{nTRACER} - \rho_{McCARD} = (1/k_{eff,McCARD} - 1/k_{eff,nTRACER})$

** Pin Power Difference: $P_{nTRACER} - P_{McCARD}$

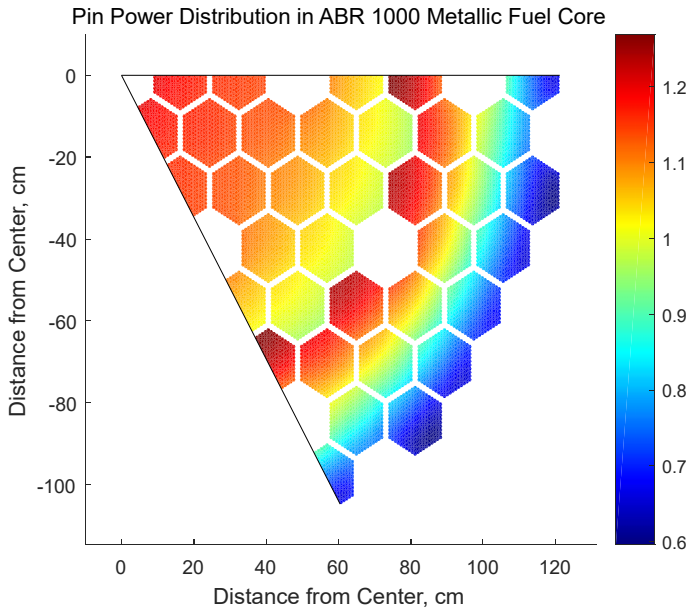

Figure 5-22. Pin Power Distribution in ABR 1000 Metallic Fuel Core from the McCARD Calculation

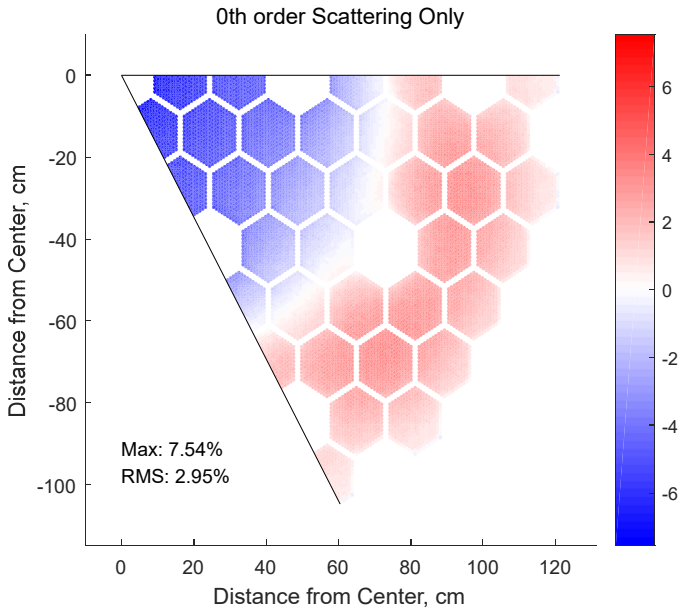

Figure 5-23. Absolute Differences in Pin Powers of nTRACER with Isotropic Scattering, Values=100*(nTRACER – McCARD)

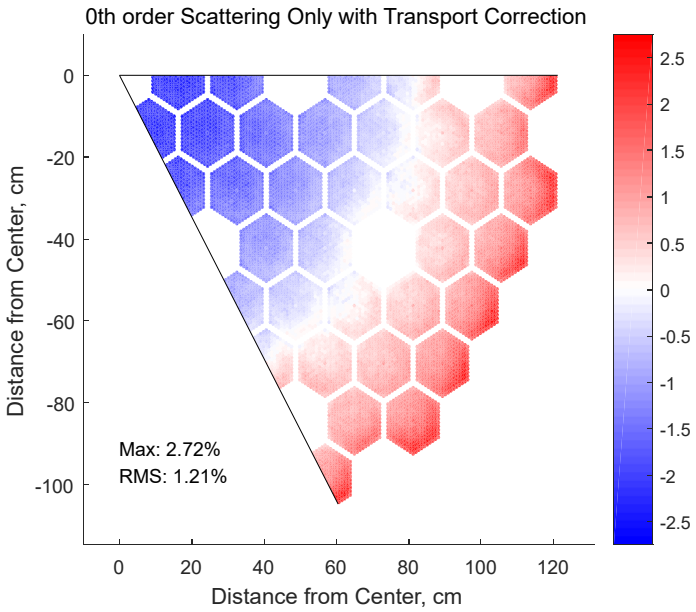

Figure 5-24. Absolute Differences in Pin Powers of nTRACER with Transport Correction, Values=100*(nTRACER – McCARD)

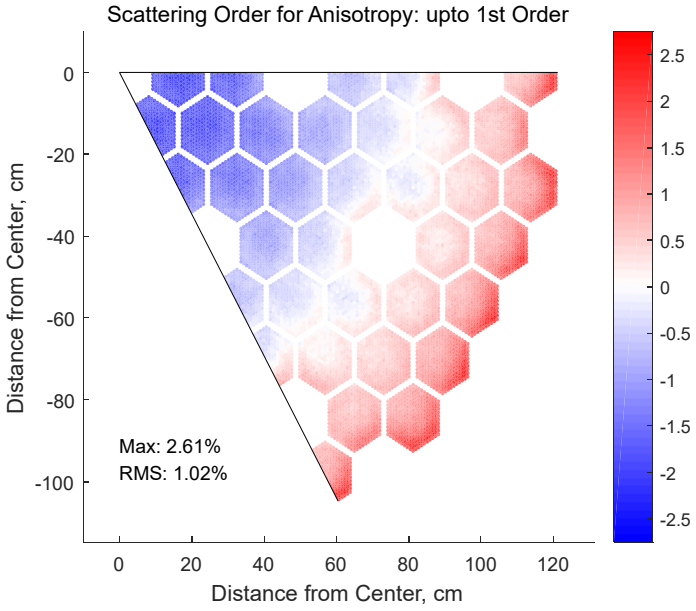

Figure 5-25. Absolute Differences in Pin Powers of nTRACER with 1st Order Anisotropic Scattering, Values=100*(nTRACER – McCARD)

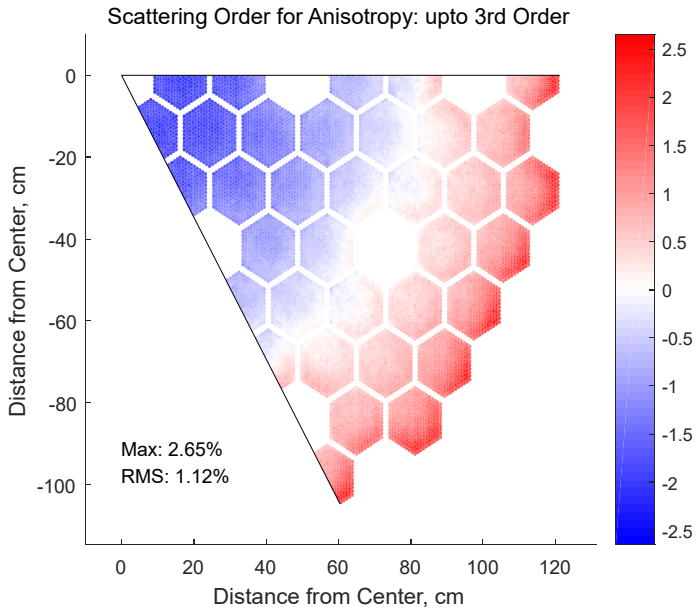

Figure 5-26. Absolute Differences in Pin Powers of nTRACER with 3rd order Anisotropic Scattering, Values=100*(nTRACER – McCARD)

5.2.4. 2D Core Calculation with Spectrum Transition Effects

To generate more accurate spectra in non-fuel assemblies and to account for spectral transition effects, a 2123G 2D core calculation was performed in EXUS-F using the hexagonal MOC module of EXUS-F. For this calculation, the explicit core configuration of homogenized assemblies was used with the vacuum boundary condition. The MOC calculation was performed with the follow parameters: 24 azimuthal angles for 180 degrees, 4 polar angles for 90 degrees and 0.1 cm ray spacing. The resulting 2123G flux solution was averaged over each assembly type and the broad group XSs were calculated for each assembly type using the corresponding average spectrum. By replacing the previous non-fuel assembly cross sections generated with single assembly calculations with the new cross sections obtained from a whole core EXUS-F calculation, the nTRACER calculation was repeated with the 3rd order anisotropic scattering treatment.

Figure 5-27 compares the neutron spectra in different

assembly types obtained from single assembly calculations with the results of the 2D EXUS-F core calculation. As can be seen, significant differences are observed in neutron spectra of non-fuel assemblies. With the spectral transition effects, the neutron spectra in control and reflector assemblies are significantly hardened because of incoming neutrons from neighboring fuel assemblies. Note that all control rods are removed, thus the control assembly positions are composed of coolant and duct. On the other hand, the spectrum in shield assembly becomes softer because of the neutrons leaking from the reflector region. The inner fuel assembly showed no noticeable difference because it is positioned in the core center region, and thus its spectrum is not compared in Figure 5-27. The neutron spectrum in the outer fuel assembly is slightly softened because of leaking-out neutrons to the reflector region, but it does not make any significant difference in the broad-group XSs.

Table 5-8 compares the multiplication factor and pin powers of nTRACER obtained with the updated non-fuel assembly XS data with the McCARD reference solutions and Figure 5-28 shows detailed pin power differences. As can be seen, the updated non-fuel assembly cross sections by considering the spectrum transition effects do not show any noticeable improvement for this problem.

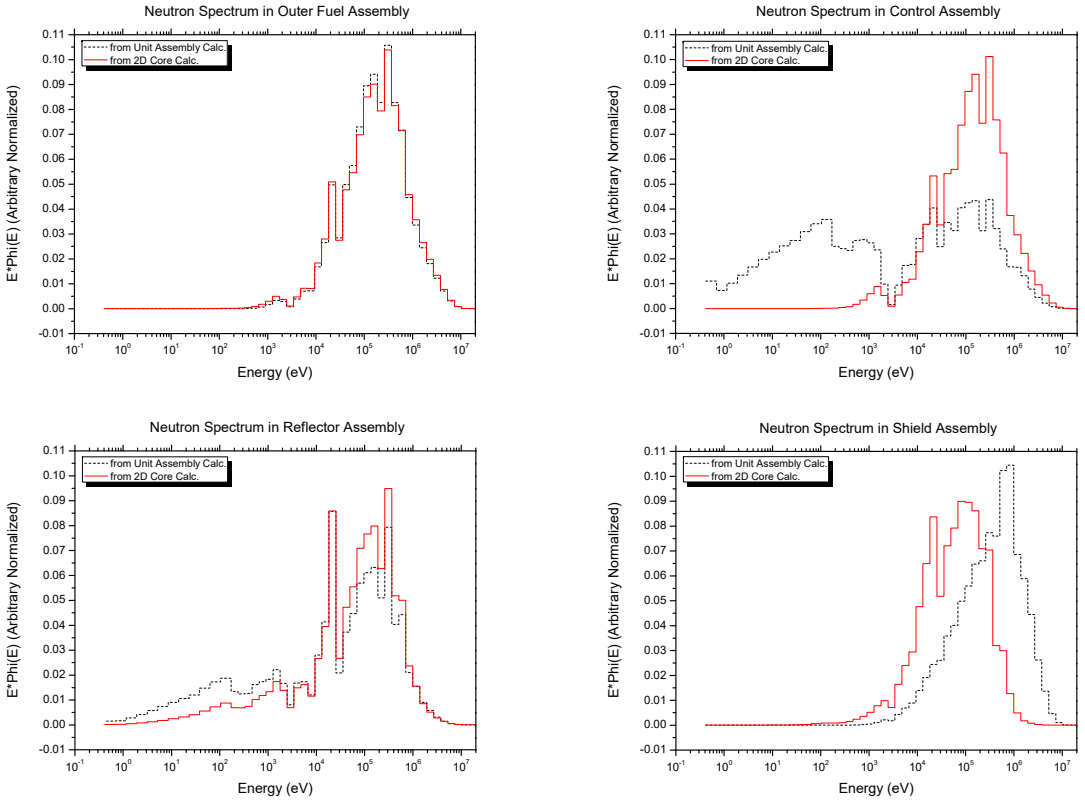

Figure 5-27. Comparison of Neutron Spectra for Outer Fuel Assembly (Top Left), Control Assembly (Top Right), Reflector Assembly (Bottom Left) and Shield Assembly (Bottom Right) Obtained from Single Assembly Calculations (black) and 2D Core Calculation (red) in EXUS-F

Table 5-8. nTRACER Results of 2D Core Problem Obtained with XSs Reflecting Spectrum Transition Effects

McCARD (Ref.)	1.21958 ± 2 pcm			
	k_{eff}	Reactivity Diff. [pcm]	Max. Pin Power Difference [%]	RMS. Pin Power Difference [%]
nTRACER	1.22372	277	2.77	1.15

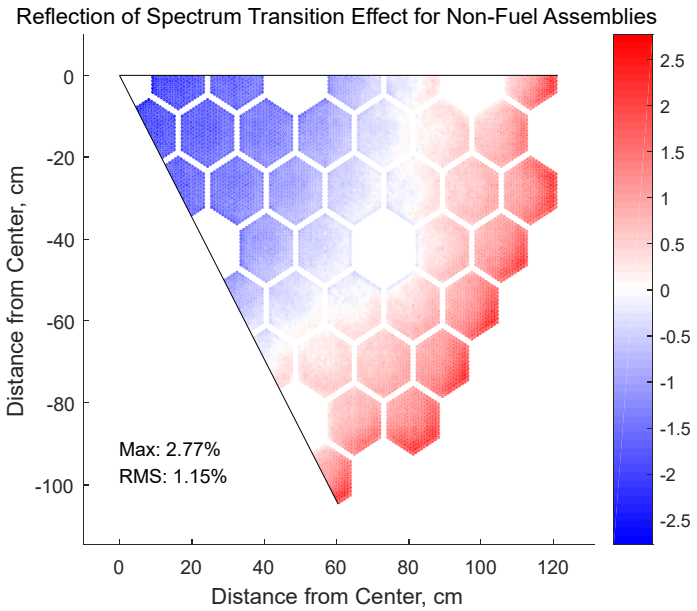

Figure 5-28. Absolute Differences in Pin Powers of nTRACER Obtained with XSs Reflecting Spectrum Transition Effects from McCARD Results

As mentioned above, the updated non-fuel assembly cross sections based on the neutron flux from the 2D core calculation have no effect on the nTRACER 2D core result. From these results, it can be stated that the spectral transition effect can be negligible for this problem set. However, the change of weighting functions of inner and outer core assemblies by the spectral transition was not considered in above results. Strictly speaking, outer core assemblies near the core/reflector boundary are most affected by the spectral transition because of incoming neutrons from reflector assemblies.

To take the spectral transition effect into account for core assemblies, 47G 2D core calculations were performed in EXUS-F. For these calculation, two sets of 47G XS data were prepared. First, EXUS-F 2D core calculation was performed with a 2123G structure and the 47G XS data (Case 1) was calculated for each single assembly using the resulting 2123G solution. The other XS data (Case 2) was prepared from the 0D mixture calculations for each assembly type. Based on two XS data set, the EXUS-F calculation was repeated with the 3^{rd} order anisotropic scattering treatment. All of the MOC calculation using EXUS_F were performed with the same condition as: 24 azimuthal angles for 180 degrees, 4 polar angles for 90 degrees and 0.1 cm ray spacing.

Table 5-9 compares the multiplication factor and pin powers of EXUS-F, obtained with the XS data from the 0D mixture calculation, with the XS data from the 2D core calculation. Figure 5-29 shows detailed assembly-wise power differences. As can be seen, the result with the XS data from the 0D mixture calculation show good agreements with the result with the XS data reflecting the spectral transition effect. It means that the spectral transition effect is not the original cause of the discrepancies of the EXUS-F/nTRACER solutions from the reference McCARD results.

Table 5-9. EXUS-F Results of 2D Core Problem Obtained with XSs w/ and w/o reflection of Spectrum Transition Effects

	k_{eff}	Reactivity Diff. [pcm]	Max. Assy Power Difference [%]	RMS. Assy Power Difference [%]
Case 1	1.21921	-	-	-
Case 2	1.21893	-19	0.25	0.12

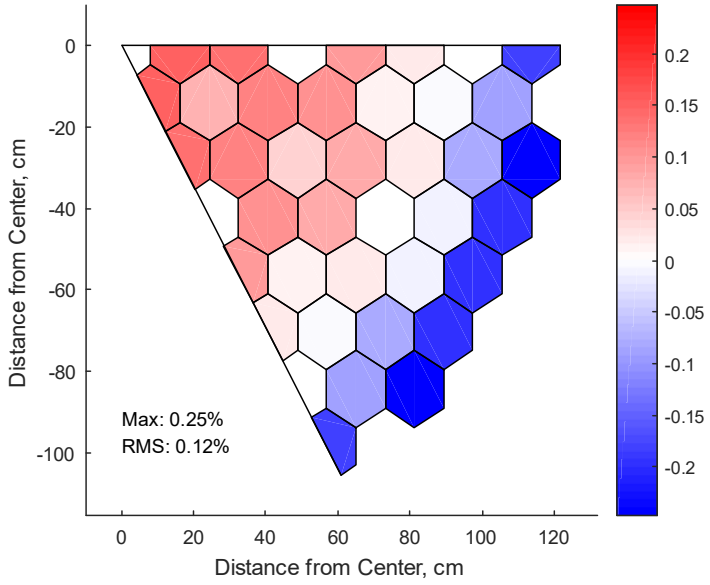

Figure 5-29. Absolute Differences in Assembly-wise Powers of EXUS-F, Values=100*(Case2-Case1)

5.2.5. 2D Core Calculation with Fine Group Structures

To investigate the main reasons for the observed discrepancies of the EXUS-F/nTRACER solutions from the reference McCARD results, different broad-group structures were studied. The broad-group structures were determined to have an equal lethargy width for all the groups above 200 eV. For lower energy range, only few groups were assigned because neutron flux is very small in the fast reactor spectrum. Table 5-10 shows the broad group structures for the ABR 1000 core calculations. For non-fuel assemblies, XS data was calculated based on the homogeneous mixture slowing down calculation for single assembly.

As shown in Table 5-11, the reactivity and pin power distribution of EXUS-F/nTRACER approaches to the McCARD reference solutions with increasing number of broad groups. With a 715G structure where each broad group contains only 2 UFGs, the reactivity difference is only 66 pcm and RMS pin power difference is 0.23%. However, the multiplication factor does not fully converge to the reference McCARD solution even with the 715G structure, as shown in Figure 5-30. These results and the results for homogeneous mixture and pin cell problems presented in Section 3 suggest that the UFG XS data such as self-shielded XSs, fission and scattering matrix are prepared well based on the ENDF format nuclear data library but the group condensation from the UFG structure to a broad group structure introduces a positive reactivity bias.

Table 5-10. Broad Group Structures for Core Calculation

Number of Broad Groups	Group Width in Number of UFGs
47	40
94	20
163	10
301	5
370	4
485	3
715	2

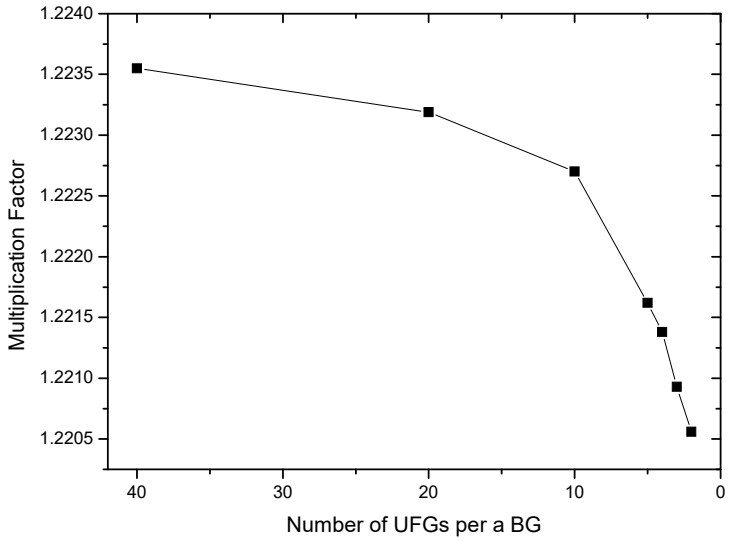

Figure 5-30. Convergence of Multiplication Factor vs. Number of Broad Group

Table 5-11. nTRACER Results of 2D Core Problem vs. Number of Broad Groups

McCARD (Ref.)	1.21958 ± 2 pcm			
nTRACER (Number of BGs)	k_{eff}	Reactivity Diff. [pcm]	Max. Pin Power Difference [%]	RMS Pin Power Difference [%]
94	1.22319	242	2.24	0.92
163	1.22270	209	1.94	0.80
301	1.22162	137	1.43	0.52
370	1.22138	121	1.29	0.44
485	1.22093	91	1.06	0.32
715	1.22056	66	0.86	0.23

5.2.6. Effects of Consistent Pn Correction

In previous part, it was observed that a large reactivity bias was introduced in the group condensation stage in EXUS-F. To investigate this problem, EXUS-F solutions were compared instead of the EXUS-F/nTRACER solution. For the comparison, a 2D core calculation in EXUS-F was performed with a 2123G XS data and a 47G XS data was prepared based on the 2123G solution. Then, the same EXUS-F calculation was repeated with the 47G XS data.

Table 5-12 shows the multiplication factors from the 2123G and 47G calculations and their discrepancies in reactivity and power difference. As can be seen, large positive reactivity difference was observed. That is to say, something was not conserved in the group condensation stage in EXUS-F and the neutron leakage may be main cause of the reactivity bias. The neutron leakage is not conserved in the group condensation without any special treatment.

To resolve this problem, the consistent Pn correction method was introduced to handle anisotropy of the total reaction. With the consistent Pn correction method, higher order moments of within group scattering XSs are corrected as below:

$$\sigma'^{l}_{s,G\to G} = \sigma^{l}_{s,G\to G} + (\sigma^{0}_{t,G} - \sigma^{l}_{t,G}) \tag{5.3}$$

where $\sigma^{l}_{s,G\to G}$ is the l-th moment within group scattering XS and $\sigma^{0}_{t,G}$ is the l-th moment total XS.

Table 5-12. Results of EXUS-F 2D Core Problems with UFG and BG XS data without reflection of Consistent Pn Correction

k_{eff} from UFG Calc.	k_{eff} from BG Calc.	Reactivity Diff. [pcm]	Max. Assy Power Difference [%]	RMS. Assy Power Difference [%]
1.21483	1.21933	304	2.45	1.30

By applying the consistent Pn correction to both of 2123G and 47G XS data, the EXUS-F 2D core calculation was repeated. Table 5-13 compares the multiplication factors and assembly power distribution from the EXUS-F calculations with the consistent Pn correction. As shown in the Table, the reactivity discrepancy between the 2123G and 47G results decreased dramatically. However, the multiplication factor in the 2123G calculation was decreased about 200 pcm by applying the consistent Pn correction method.

The EXUS-F/nTRACER calculation was performed for 2D core calculation with the consistent Pn corrected 47G XS data. The same calculation parameters were used with the previous calculations. Table 5-14 compares the multiplication factor and pin powers of nTRACER obtained with the updated non-fuel assembly XS data with the McCARD reference solutions and Figure 5-31 shows detailed pin power differences. As can be seen, the consistent Pn correction made nTRACER results worse. The reactivity difference from the McCARD reference was changed from 266 pcm to -426 pcm and the pin power differences was also slightly increased. About this problem, further study is required to identify the reason for this phenomena and the leakage conservation in the group condensation.

Table 5-13. Results of EXUS-F 2D Core Problems with UFG and BG XS data with reflection of Consistent Pn Correction

k_{eff} from UFG Calc.	k_{eff} from BG Calc.	Reactivity Diff. [pcm]	Max. Assy Power Difference [%]	RMS. Assy Power Difference [%]
1.21275	1.21213	-42	0.66	0.44

Table 5-14. nTRACER Results of 2D Core Problem Obtained with Consistent Pn Correctd XS

McCARD (Ref.)	1.21958 ± 2 pcm			
	k_{eff}	Reactivity Diff. [pcm]	Max. Pin Power Difference [%]	RMS. Pin Power Difference [%]
nTRACER	1328	−426	2.96	1.49

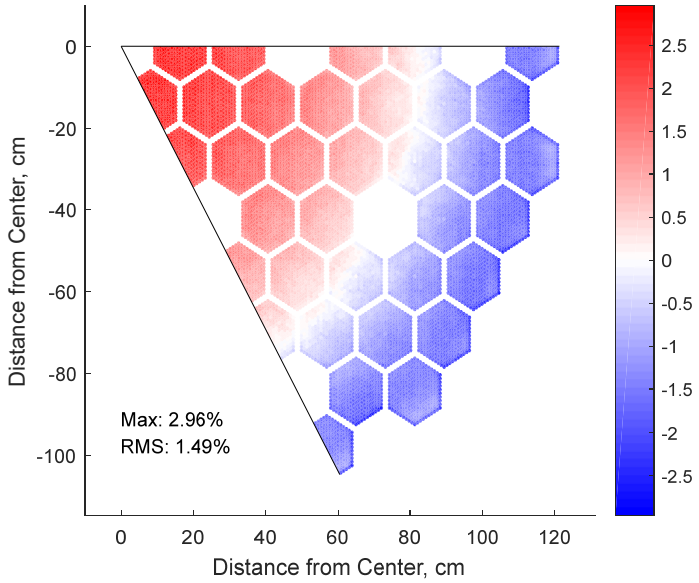

Figure 5-31. Absolute Differences in Pin Powers of nTRACER Obtained with Consistent Pn Correctd XS

5.2.7. Effects of Different Nuclear Data Evaluations

To verify the capability of processing general ENDF format nuclear data libraries, the 2D core problem was repeated with the cross sections based on the ENDF/B-VII.1 and JENDL 4.0 libraries. The probability tables were prepared using the PURR module of NJOY, but other data were processed directly in EXUS-F. To generate the MG XS in EXUS-F, the assembly model was used for fuel assemblies and the homogeneous mixture calculations were performed for non-fuel assemblies with the aforementioned 47G structure. Reference solutions were obtained from the McCARD calculations based on the continuous energy ENDF/B-VII.1 and JENDL 4.0 libraries with 200,000 particles per cycle, 2,000 active cycles and 500 inactive cycles.

Table 5-15 compares the multiplication factors and pin powers of nTRACER and McCARD calculations with the ENDF/B-VII.1 and JENDL 4.0 libraries. The McCARD multiplication factor obtained with the JENDL 4.0 library is 481 pcm larger than that obtained with the ENDF/B-VII.1 library. Similarly, nTRACER multiplication factor with JENDEL 4.0 is 472 pcm larger than that with ENDF/B-VII.1. The reactivity differences and pin power differences obtained with the ENDF/B-VII.1 and JENDL 4.0 libraries are very similar with the values obtained with the ENDF/B-VII.0 library. As shown in Figure 5-32 and Figure 5-33, the results obtained with the ENDF/B-VII.1 and JENDL 4.0 libraries show the global power tilt observed with the ENDF/B-VII.0 library.

Table 5-15. nTRACER Results of 2D Core Problem vs. Different Nuclear Data Libraries

McCARD (Ref.)	ENDF/B-VII.1: 1.21917 ± 2 pcm JENDL 4.0: 1.22398 ± 2 pcm			
nTRACER (Nuclear Data Library)	k_{eff}	Reactivity Diff. [pcm]	Max. Pin Power Difference [%]	RMS. Pin Power Difference [%]
ENDF/B-VII.1	1.22339	283	2.63	1.18
JENDL 4.0	1.22811	275	2.63	1.17

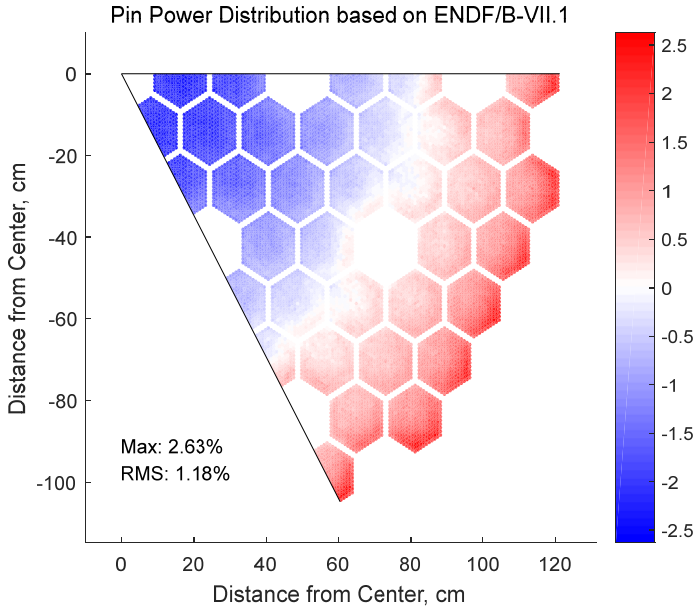

Figure 5-32. Absolute Differences in Pin Powers between nTRACER and McCARD Obtained with ENDF/B-VII.1

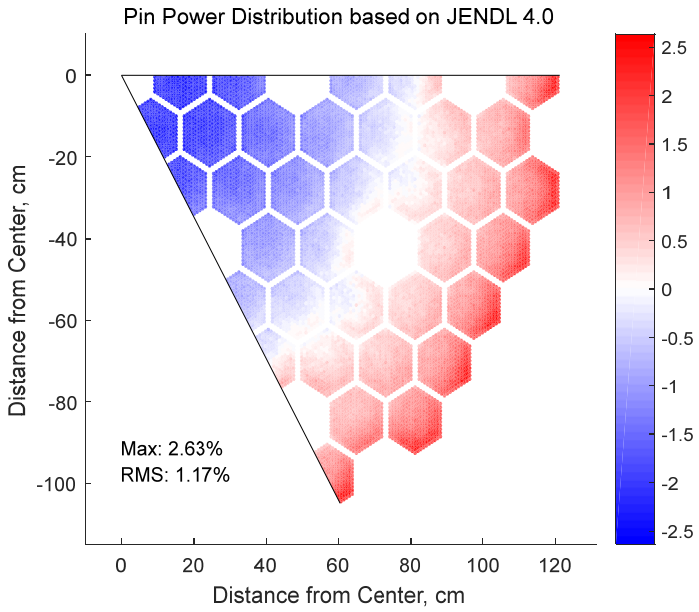

Figure 5-33. Absolute Differences in Pin Powers between nTRACER and McCARD Obtained with JENDL 4.0

Chapter 6. Conclusion

A multigroup cross section generation code EXUS-F was developed to generate the multigroup XSs for fast reactor analysis It was developed such that it can process the ENDF files directly without requiring any advance generation of ultrafine group XS data as the MC2-3 and ECCO do. The RECONR module of the NJOY system was introduced to prepare the pointwise XS from the resonance data in the ENDF format nuclear data libraries and the Doppler broadening effect was incorporated by the internal functions implementing the SIGMA1 method and the Gauss-Hermite quadrature. It turned out that the Gauss-Hermite module can reduce the computing time significantly and thus it was used for the heavy nuclides. The self-shielding effect in the ultrafine group XS was incorporated based on the pointwise XSs for entire energy range except the unresolved resonance range. For the self-shielding in unresolved resonance range, the method based on the pre-generated probability table library was used. The functions to calculate the fission matrices and the scattering transfer matrices directly from the ENDF format nuclear data library were realized. The scattering matrices for higher order moments are obtained up to user specified order not only for elastic scattering, but also for inelastic scattering and *(n,xn)* reactions. An ultrafine group structure consisting of 2123 energy groups ranging upto 20 MeV is employed for the spectrum calculation and the ultrafine group structure can be adjusted by the user input. The extended transport approximation was applied to perform the 0D calculations to obtain the high order moment neutron spectra and the solver for cylindrical geometry based on the Collision probability method was implemented. The MOC transport solver for hexagonal geometry with the high order scattering treatment capability was also implemented. The spectral transition effect was considered using the MOC transport solver.

To verify EXUS-F, the McCARD and EXUS-F calculations were performed using two different nuclear data libraries, ENDF/B-VII.0 and JENDL 4.0 for two problems sets: 0D mixture problems and cylinder approximate pin problems which were constructed based on the fuel assembly of the ABR 1000 benchmark. In the 0D mixture problems with both libraries, the infinite multiplication factors of EUXS-F were matched well with McCARD within 60 pcm reactivity difference. The group condensed neutron spectrum and total XSs of Fe-56 and Cr-52 also show very good agreements with McCARD in the 0D mixture problem. In the cylindrical problems, similar results were observed in the multiplication factor, the group condensed spectrum and total XSs.

The EXUS-F/nTRACER calculations were performed for the ABR 1000 metallic fuel core problem simplified from three dimensional to two dimensional to test the EXUS-F/nTRACER system for the fast reactor analysis based on the ENDF/B-VII.0 library. The approximate cylindrical fuel assembly model for EXUS-F was introduced based on the continuous energy Monte Carlo solutions and the approximate model gave very similar group condensed XSs compared with the values from the explicit geometry. The multiplication factors for two assembly problems from the EXUS-F/nTRACER calculations agreed well with the McCARD results within 20 pcm reactivity differences. In the 2D core problem, nTRACER estimated the multiplication factor and the pin power distribution based on the 47G XS data from EXUS-F without considering the spectral transition effect with 250 pcm reactivity difference and 1.1% RMS. Error, respectively. The spectrum transition effect was reflected on the MG XS generation by performing the 2D core calculation using the MOC solver of EXUS-F, but it did not make a change in the EXUS-F and nTRACER results. By using the fine group structure, the 715 G structure, nTRACER gave better result with 66 pcm reactivity difference and 0.23% RMS pin power difference. Positive reactivity bias about 300 pcm was introduced in the group condensation in EXUS-F, but it was resolved by introducing the consistent Pn

correction method. However, the correction method made the EXUS-F/nTRACER results worse. The EXUS-F/nTRACER calculations were performed for the 2D core calculation using the ENDF/B-VII.1 and the JENDL 4.0 libraries. Results using the different nuclear data libraries were very similar with the results based on the ENDF/B-VII.0 library.

Although the EXUS-F/nTRACER system using the 47G structure overestimated the multiplication factor about 260 pcm and the power tilt was observed with 1.1% RMS. difference in the 2D ABR core problem, the values may be admissible. And the nTRACER show excellent agreements in the assembly problems with the 47G structure and also give better results with the fine group structures for the 2D core problem. It can thus be stated that EXUS-F works properly to prepare the UFG XSs and generate the MG XSs by performing the UFG transport calculations. The versatility of EXUS-F which can use any nuclear data set as long as the set is given in the ENDF format was proved useful by the test of three different nuclear data libraries.

As future work, further research will be conducted about the problem to make results worth with the broad group structure in the 2D core problem and the performance of the EXUS-F/nTRACER system for the 3D core calculation will be tested.

Reference

1. Y. S. Jung, C. B. Shim, C. H. Lim and H. G. Joo, "Practical numerical reactor employing direct whole core neutron transport and subchannel thermal/hydraulic solver," Annals of Nuclear Energy, 62, 357-374 (2013).
2. J. Yoo et al, "Overall System Description and Safety Characteristics of Prototype Gen IV Sodium Cooled Fast Reactor in Korea," Nuclear Engineering and Technology 48, 1059-1070 (2016).
3. W. S. Yang, "Fast Reactor Physics and Computational Methods," Nuclear Engineering and technology, 44, 107 (2012).
4. I. I. Bondarenko, et al, "Group Constants for Nuclear Reactor calculation," Consultants Bureau Enterprises, Inc., New York (1964).
5. B. J. Toppel, H. Henryson II, and C. G. Stenberg, "ETOE-2/MC^2-2/SDX Multi-group Cross-Section Processing," Conf-780334-5, Proc. Of RSIC Seminar-Workshop on Multi-group Cross Sections, Oak Ridge, TN (1978).
6. G. Rimpault, "Algorithmic features of the ECCO cell code for treating heterogeneous fast reactor subassemblies," International Topical Meeting on Reactor Physics and Computations, Portland, Oregon, May 1-5 (1995).
7. T. HAZAMA et al, "Development of a Fine and Ultra-Fine Group Cell Calculation Code SLAROM-UF for Fast Reactor Analyses," Journal of Nuclear Science and Technology, 43, 8 (2006).
8. C. H. Lee, W. S. Yang, "MC^2-3: Multigroup Cross Section Generation Code for Fast Reactor Analysis," ANL-NE-11-41, Argonne National Laboratory (2011).
9. R. E. MacFarlane and D. W. Muir, "The NJOY Nuclear Data Processing System Version 91," LA-12740-M, Los Alamos

National Laboratory (1994).
10. C. R. Weisbin et al, “MINX: A Multigroup Interpretation of Nuclear X-Section from ENDF/B,” LA-6486-MS, Los Alamos Scientific Laboratory (1976).
11. W. J. Davis, M. B. Yarbrough, and A. B. Bortz, “SPHINX, A One-Dimensional Diffusion and Transport Nuclear Cross Section Processing Code,” WAPD-XS-3045-17, Westinghouse (1977).
12. R. B. Kidman, R. E. MacFarlane, “LIB-VI, A Library Group Constants for Nuclear Reactor Calculations,” LA-6260-MS (1976)
13. H. Takano et al., “JAERI Fast Reactor Group Constants Set, Version 2.,” JAERI 1255 (1978)
14. J. D. Kim and C. S. Gil, “Development and Benchmark of Multi-group Library for Fast Reactor Using JEF-2.2,” KAERI/TR-842/97 (Korean) (1997)
15. D. E. Cullen, “Program SIGMA1 (Version 74-1),” Lawrence Livermore Laboratory report UCID-16426 (1974).
16. Dean C, Perry R, Neal R, Kyrieleis A, “Validation of Run-time Doppler Broadening in MONK with JEFF3.1,” J. Korean Phys. Soc., 59, 2, 1162 (2011).
17. R. E. MacFarlane, “TRANSX 2: A Code for Interfacing MATXS Cross-Section Libraries to Nuclear Transport codes,” LA-12312-MS, Los Alamos National Laboratory (1992).
18. R. D. MOSTELLER and R. C. LITTLE, “Impact of MCNP Unresolved Resonance Probability-Table Treatment on Uranium and Plutonium Benchmark,” Trans. of ANS. 79, 313 (1998).
19. C. Lim, H. G. Joo and W. S. Yang, “Applications of the Probability Table on Deterministic Coe for Unresolved Resonance Self-shielding,” Transactions of the American Nuclear Society Winter Meeting, Washington, U.S, Oct 29 – Nov 2 (2017).

20. R. J. J. Stamm'ler, M. J. Abbate, "Methods of Steady-State Reactor Physics in Nuclear Design", Academic Press, London, 105-139 (1983).
21. Min Ryu et al., "Incorporation of Anisotropic Scattering in nTRACER," Korea Nuclear Society Autumn Meeting, Pyeongchang, Korea, Oct 29-31 (2014).
22. T. K. Kim, et al, "Core design studies for a 1000 MWth advanced burner reactor," Annals of Nuclear Energy (2009).
23. H. J. Shim, et al, "McCARD: Monte Carlo Code for Advanced Reactor Design and Analysis," Nuclear Engineering and Technology, 44, 161-176 (2012).

초 록

본 연구에서는 고속로 해석을 위한 다군 군정수 생산 코드 EXUS-F를 개발하였다. 이 코드는 고속로 중성자속 분포에 뚜렷하게 나타나는 중간 물질 핵종들의 공명 자기 차폐 효과(Self-shielding effect)를 고려하기 위해 초미세군 중성자속 계산 방법을 기반으로 한다. ENDF-6 형식으로 주어지는 평가핵자료집으로부터 직접 군정수 생산을 위해 평가핵자료집 후처리 코드 NJOY 체계의 RECONR 모듈이 도입되었다. 분해 공명(Resolved resonance), 비분해 공명(Unresolved resoancne) 및 고에너지에 존재하는 중간 무게 핵종들의 공명들에 의한 자기 차폐 효과를 처리 할 수 있는 방법을 구현하였다. 비분해 공명 영역 내 자기 차폐 효과를 처리 하기 위해 사전에 생산된 확률표(Probability Table) 라이브러리에 기반하는 확률표 방법을 제안하였다. 평가핵자료집 내 자료로부터 핵분열 스펙트럼 행렬 및 중성자 산란 행렬을 직접 계산하는 기능을 구현하였다. 0차원 초미세군 감속 계산 시 고차 중성자속 모먼트를 얻기 위해 N차 확장 수송 보정법을 도입하고, 중성자의 자유로운 이동에 의한 누설 효과를 고려하기 위해 충돌확률법(Collision Probability)과 특성곡선법(Method of Characteristics, MOC)을 적용하여 1차원 실린더 구조 및 고속로의 육각형 노심 구조에 대한 수송 계산 기능을 도입하였다. 특히 특성곡선법 고려 시 중성자의 비등방성 산란을 고려하기 위한 고차 산란 선원 방법을 구현하였다.

코드의 검증을 위해 ABR 1000 벤치마크의 집합체 구조로부터 0차원 혼합물 및 1차원 실린더 문제 세트를 구성하고, EXUS-F 코드를 이용해 초미세군 계산을 수행하고, 서울대학교의 몬테칼로 코드 McCARD로부터 얻은 계산 결과와 비교하였다. 비교 결과 초미세군 반응 단면적 및 해당 반응 단면적들로부터 얻은 다군 반응단면적이 정상적으로 생산됨을 확인하였다. ENDF/B-VII.0 평가핵 자료집을 이용하여 생산된 다

군 반응단면적의 건전성을 평가하기 위해 직접 전노심 수송계산 코드 nTRACER를 이용하여 2차원 ABR 1000 노심 문제에 대한 계산을 수행하였다. 계산 결과 몬테칼로 결과와 반응도 오차 260 pcm, 봉단위 출력 RMS 오차 1.1% 이내로 잘 맞음을 확인하였다. 동일한 계산을 JENDL 및 ENDF/B-VII.1 핵자료 라이브러리로 수행한 결과 ENDF/B-VII.0 계산 결과와 동일한 경향을 가짐을 확인하였고, 이를 통해 EXUS-F 코드가 ENDF-6 형식의 핵평가자료집을 잘 처리함을 확인하였다.

Keywords : 다군 반응단면적
고속로
초미세군
ENDF 형식
ABR1000 벤치마크
Student Number : 2012-30964

감사의 글

학부 3학년, 원자력 대학생 논문 연구를 계기로 원자로물리연구실에 들어온 지 9년만에 박사 학위를 받으며 졸업하게 되었습니다. 살아오면서 가장 오랜 기간 동안 연구실에 적을 두고 지내면서, 포기하고 싶은 적도 많았지만 감사하게도 많은 분들의 도움을 받아 여기까지 올 수 있었습니다. 그 중에서도 오랜 기간 동안 여러모로 많이 부족한 저를 지도해주신 제 지도 교수님, 주한규 교수님께 가장 큰 감사를 드립니다. 학부 시절, 교수님이 강의하신 원자로 물리 수업을 듣고 학업에 뜻을 세울 수 있었고, 긴 연구실 생활 동안 교수님의 정성어린 지도 덕분에 조금이나마 성장할 수 있었습니다. 또한 학위 심사 및 논문 작성 과정에서 많은 이해와 지도 덕분에 무사히 졸업 하게 되었습니다. 다시 한 번 감사드립니다.

다음으로 바쁜 와중에도 흔쾌히 논문 심사를 맡아 주시고, 많은 관심과 조언을 주신 심형진 교수님, 김응수 교수님, 김상지 박사님, 이영욱 박사님께 감사드립니다. 다양한 경험에서 나오는 심사 위원님들의 조언 덕분에 학위 논문의 완성도를 높일 수 있었습니다.

이 연구를 진행하는 데 많은 조언과 도움을 주시고, 짧지 않은 미국 연수기간 동안 물심양면으로 도와주신 Michigan 대학교의 양원식 교수님께도 진심으로 감사드립니다.

원자로물리연구실로 인해 인연을 맺게 된 선배, 동기 및 후배님들에게도 감사하다는 말을 전하고 싶습니다. 연구실에 갓 들어왔을 때부터 많은 조언을 해주시고 훌륭한 선배의 귀감이 되어주신 동욱이형, 동규형, 민재형, 주일이형, 호진이형, 관영이형, 무훈이형, 은현이형, 연상이형에게 감사의 말씀을 드립니다. 또한 오랜기간 연구실 생활을 같이 하면서 도움을 준 천보, 범우, 채호, 희정, 한솔이형, 재진, 민, 영석, 기범, 현식, 현호, 준호형에게 고맙다는 말을 전하고 싶습니다. 또한 준수, 남재, 승욱, 소리, 승엽, 준택, Alberto, Jorge에게도 감사함을 전하며, 남은 기간

동안 훌륭한 연구를 수행하여 무사히 학위를 마치기를 기원합니다.

긴 대학 생활 동안 옆에서 묵묵히 기도하고 응원해준 사랑하는 어머니, 승현, 지은에게도 감사한 마을을 전하고 싶습니다. 힘든 시절 가족들의 응원 덕분에 이겨낼 수 있었습니다. 또한 학위 기간동안 옆에서 조언 및 지지를 해주신 큰 아버지, 작은아버지 두분 및 일가 친척 분들에게도 감사를 전합니다.

마지막으로 살아 계셨다면 누구보다 기뻐하셨을 사랑하는 아버지께 이 논문을 바칩니다.